molecular pharmaceutics

pubs.acs.org/molecularpharmaceutics

Article

Nattokinase Encapsulated Nanomedicine for Targeted Thrombolysis: Development, Improved *in Vivo* Thrombolytic Effects, and Ultrasound/Photoacoustic Imaging

Vishnu Priya, Samridhi, Nitesh Singh, Debabrata Dash, and Madaswamy S. Muthu*

Cite This: *Mol. Pharmaceutics* 2024, 21, 283−302

Read Online

ACCESS | Metrics & More | Article Recommendations | Supporting Information

ABSTRACT: Nattokinase (NK), a potent thrombolytic enzyme that dissolves blood clots, is highly used in the treatment of cardiovascular disorders. However, its effective delivery remains demanding because of stability and bioavailability problems owing to its high molecular weight and proteineous nature. In this research, we have developed novel NK-loaded nontargeted liposomes (NK-LS) and targeted liposomes (RGD-NK-LS and AM-NK-LS) by the reverse phase evaporation method. The physiochemical characterizations (particle size, polydispersity index, zeta potential, and morphology) were performed by a Zetasizer, SEM, TEM, and AFM. The Bradford assay and XPS analysis confirmed the successful surface conjugation of the targeting ligands. Platelet interaction studies by CLSM, photon imager optima, and flow cytometry showed significantly higher ($P < 0.05$) platelet binding affinity of targeted liposomes. *In vitro* evaluations were performed using human blood and a fibrinolysis study by CLSM imaging demonstrating the potent antithrombotic efficacy of AM-NK-LS. Furthermore, bleeding and clotting time studies revealed that the targeted liposomes were free from any bleeding complications. Moreover, the *in vivo* $FeCl_3$ model on Sprague−Dawley (SD) rats using a Doppler flow meter and ultrasound/photoacoustic imaging indicated the increased % thrombolysis and potent affinity of targeted liposomes toward the thrombus site. Additionally, *in vitro* hemocompatibility and histopathology studies demonstrated the safety and biocompatibility of the nanoformulations.

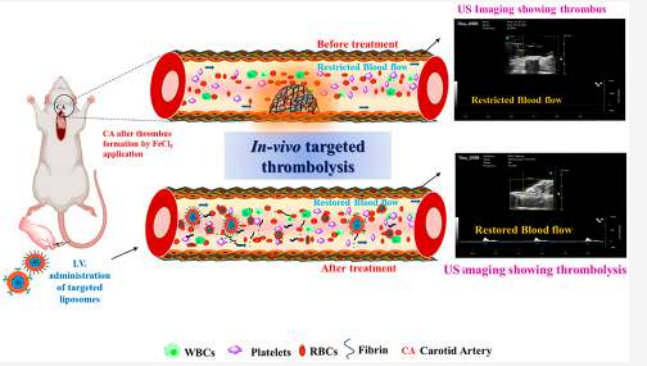

KEYWORDS: *Nattokinase, thrombolysis, fibrinolysis, thrombus targeting, photoacoustic imaging*

1. INTRODUCTION

Maintaining healthy circulation is an essential tool to sustain cardiovascular health. Preservation of healthy circulation is one of the critical parameters in maintaining cardiovascular activities. According to the WHO, cardiovascular diseases (CVDs) remain a principal reason for death worldwide and affect millions of lives with associated risk and disorders.[1] At present, the risk to experience CVDs is even more due to an unhealthy lifestyle, use of tobacco, consumption of alcohol, and insufficient physical activity. Other than this, some physiological features such as hypertension, high blood glucose, and high blood cholesterol levels also contribute to originating CVDs.[2] The CVDs are mainly a group of disorders that include diseases related to the heart and blood vessels. One of the primary causes that is responsible for the induction of these diseases is the development of the thrombus inside the vesicular system that leads the way to a heart attack or stroke. In normal hemostasis, when the blood vessels are damaged or ruptured, the development of a thrombus or clot is an ordinary process to stop the bleeding and allows the body to self-repair from the injury. However, the formation of a thrombus in the circulatory system without any injury (thrombosis) can cause life-threatening conditions such as myocardial infarction, ischemic cardiac damage, and thromboembolism.[3]

Currently, prompt revascularization provides an initial therapeutic alternatives utilizing a pair of reliable methods of angioplasty and the surgical removal of obstructions in a blood vessel. In contrast, for these operative procedures, patient must be shifted to a specialized medical facility to undergo cardiac surgery in order to carry out these intervention processes.[4] In addition to these, a variety of antithrombotic medications, including anticoagulants (heparin, warfarin, other thrombin inhibitors, and factor Xa inhibitors), antiplatelets (abciximab), and thrombolytics (streptokinase, nattokinase, and lumbroki-

Received: September 11, 2023
Revised: November 23, 2023
Accepted: November 28, 2023
Published: December 21, 2023

nase), are clinically offered for the management of thrombotic diseases.[5] The majority of such medications has a number of drawbacks and side effects, including a shorter half-life, a narrow therapeutic window, and limited targeting ability, demands higher dosing with therapeutic monitoring, and can cause life-threatening hemorrhagic complications.[6] Therefore, there is a great need to create a system that can deliver these antithrombotic medications in a safe and efficient manner. Natto is a type of vegetable cheese produced by fermenting soybeans with the nonpathogenic bacteria Bacillus natto. NK, an enzyme formed during this fermentation process, has been extensively investigated for use in promoting arterial and cardiovascular wellness.[7] NK comes under the category of serine endopeptidase and is composed of 275 amino acids. It has been proven that NK has potent fibrinolytic activity compared to any known enzyme, confirmed by laboratory tests.[8]

Fibrinolysis is an ordinary physiological process that aids in wound healing and plays a crucial role in maintaining or restoring the blood flow after hemostasis. The major organs of the body are constantly provided with the oxygen, nutrients, and other products they require for optimal functioning owing to the proper regulation of fibrinolysis, which helps to maintain healthy blood flow through the vascular system. NK is a novel generation of thrombolytic medication with a significant fibrinolytic activity. It can increase the levels of an endogenous fibrinolytic enzyme by activating a plasminogen activator in addition to directly acting on fibrinolysin. NK has benefits over other thrombolytic medications, including low toxicity, easy production, and cheap cost.[9] Furthermore, it can be administered orally and via injection to dissolve the thrombus. It is also readily absorbed by the body. Despite this, NK is sensitive to losing biological activity after being administered to the body and prone to changes in the external environment, particularly changes in terms of temperature and pH.[10] Therefore, in order to increase its stability and targeting, delivery methods of NK are currently being developed and extensively researched.

Targeting the delivery of these thrombolytic agents to a localized disease area has drawn growing interest in the area of nanotechnology over the past ten years to resolve these issues and improve therapeutic efficacy. The yield and thrombolytic activity of NK are growing at present as the fermentation process has been progressively optimized with technological advancements. A novel approach to encapsulate NK could be developed to utilize NK's activity along with its adequate delivery as a thrombolytic drug. In order to preserve NK, Hsieh et al. (2009) used Na-PGA (polyglutamic acid) as a coating material and discovered that the microencapsulated NK had greater stability for temperature and pH than the free form.[11] Additionally, NK immobilization on polyhydroxybutyrate (PHB) nanoparticles increased the enzyme's activity by 20%.[12]

A liposome is a mainly double bilayer membrane resembling the cell membrane structure and features. The toxicity and immunogenicity of liposomes were found to be minimal in terms of biodegradability and compatibility with the organism.[13] For encapsulating bioactive substances, liposomes have recently been extensively used in the fields of food and pharmaceuticals. In a liposome, cholesterol typically functions as a component that gives the membranes rigidity and enhances the characteristics of the bilayer membranes.[14] Liposomal vesicles have been demonstrated to be potential nanocarriers for targeted therapy owing to its bilayer phospholipid constitution which is nonimmunogenic, nontoxic, and biocompatible in nature.[15] In addition to having these characteristics, they are considered to be appealing nanocarriers for both hydrophobic and hydrophilic drugs. Furthermore, liposomes allow surface modification for stealth action and improve the targeting efficacy for the site-specific delivery of drugs. Additionally, several liposomal preparations of anticancer therapeutics have received regulatory approval for parenteral administration.[16] These characteristics of liposomes allow them to be ideal nanocarriers for applications involving drug delivery. A large number of researchers previously worked on and are currently working on the development of thrombus-targeted liposomal formulations, which have been identified as an appropriate nanocarrier for the delivery of antithrombotic drugs. NK delivery via a liposomal carrier can address stability-related problems and enhance bioavailability, resulting in potent biological activity.[17] However, by employing suitable methods, site specificity and prolonged activity can be achieved. Additionally, to enhance the course of treatment, it is also essential to lessen several other challenges associated with drug delivery of antithrombotics, such as lack of drug accessibility to the thrombus, drug denaturation in plasma, rapid drug clearance, bleeding complications, and a variety of adverse effects.[18]

Since liposomes have a major drawback related to half-life and instability in the circulatory system, addressing these limitations solely through the delivery method is insufficient. Targeted drug delivery systems may offer a superior solution to get around all related drawbacks and could provide a drug delivery tool to increase therapeutic outcomes while minimizing side effects. Improved stability and controlled drug release for a prolonged period of time can be achieved by targeted or modified liposomal systems, which also enhance the drugs' bioavailability to the targeted organ or tissue location and avoid the distribution of drugs to nontargeted areas that induce side effects. Additionally, their physical characteristics, such as their lesser dimensions, small size range, and special biocompatibility, increase the extent of their use clinically.[19]

Earlier studies have extensively investigated the use of D-tocopheryl polyethylene glycol 1000 succinate monoester (TPGS) in the development of drug delivery systems considering their application in a variety of purposes, such as for stabilizing, emulsifying, solubilizing, enhancing diffusion, wetting, spreading, etc.[20] NK-loaded liposomes utilizing TPGS can improve encapsulation efficiency, stability, targeting, and half-life, which may further increase therapeutic potential.[21]

The activation of platelets, which are essential for the development of thrombin generation, changes the conformation of the GPIIb/IIIa receptors, which are widely distributed on activated platelets, and makes them stimulated. As a result, hemostasis pathways can continue to function while its ligand, fibrinogen, is in the bound state.[22] Targeted delivery of antithrombotic medicines can be achieved by conjugating monoclonal antibodies (MABs) or selective peptides that inhibit or antagonize these receptors. In this article, arginyl-glycyl-aspartic acid (RGD), a small tripeptide, and abciximab (AM), a chimeric human monoclonal antibody, were used as a targeting moiety to interact with activated GPIIb/IIIa integrin receptors available at the thrombus site. In prior research, RGD-decorated liposomes were demonstrated to have a higher affinity for activated platelets. Furthermore, AM is a clinically used antiplatelet drug that has been approved for its ability to inhibit GPIIb/IIIa.[23,24]

In order to significantly improve the antithrombotic treatment, here, we designed RGD- and AM-decorated targeted liposomes for NK delivery. A reverse phase evaporation

https://doi.org/10.1021/acs.molpharmaceut.3c00830
Mol. Pharmaceutics 2024, 21, 283−302

technique was used to fabricate the liposomes, either with or without a targeting moiety. Physical characteristics such as size of the particle, PDI, shape, zeta potential, the efficiency of drug encapsulation, thermal stability, and surface chemistry were then determined for these liposomes. Moreover, *in vitro* studies (such as drug release, activated partial thromboplastin time (aPTT), prothrombin time (PT), % clot lysis, clot targeting affinity, hemocompatibility, *in vitro* imaging, flow cytometry, and thrombolysis by CLSM) and *in vivo* studies (bleeding time study, clotting time study, $FeCl_3$ induced thrombosis model, ultrasound imaging, photoacoustic imaging, and histopathology) were carried out to investigate its potency and efficacy.

2. MATERIALS AND METHODS

2.1. Materials. Nattokinase was a generous gift from Zytex Biotech Pvt. Ltd., Mumbai. *N*-Hydroxysuccinimide (NHS) and ethyl (dimethylaminopropyl)carbodiimide (EDC) were obtained from Sisco Research Laboratories Pvt. Ltd., Mumbai, India. Soya phosphotidylcholine (HSPC) was a considerate gift provided by Lipoid GmBH, Germany. TPGS, fibrinogen from human plasma, RGD peptide, thrombin from bovine plasma, and coumarin-6 were purchased from Sigma-Aldrich (St. Louis, MO, USA). Phosphoplastin RL and phospholine ES were generously gifted by R2 Diagnostic Inc., Indiana, USA. Cholesterol was obtained from Central Drug House, New Delhi, India. Abcixirel was purchased from Reliance Life Sciences Pvt. Ltd., Navi Mumbai, India. Ferric chloride and Alexafluor 488 fibrinogen were procured from Thermo Fischer Scientific, CA, USA. Fetal bovine serum (FBS) was purchased from Gibco Life Technologies (AG, Switzerland). Calcium chloride was purchased from Central Drug House (P) Ltd., New Delhi, India. All solvents, such as chloroform and methanol, were of high performance liquid chromatography (HPLC) grade. All chemicals were used without further purification. Millipore water was prepared with a LAB-JAL Milli-Q System.

2.2. Methods. *2.2.1. Preparation of Nontargeted and Targeted Liposomes.* The reverse phase evaporation technique was used for the preparation of liposomes. The thrombolytic drug, i.e., NK-loaded liposomes, was fabricated by using TPGS (nontargeted) and TPGS-COOH (targeted) with a slight modification. Here, hydrogenated soya phosphatidylcholine (HSPC), cholesterol (CHOL), TPGS, and TPGS-COOH were dissolved in chloroform in a beaker. The aqueous media were then added at the same volume in the above mixture and allowed for probe sonication for 40 s. The obtained emulsion was transferred to a round-bottom flask (RBF). The RBF was then attached to a rotary evaporator (IKA, China) and allowed to rotate at 70 rpm. The temperature was maintained at 65 °C, and the organic solvent was removed by slow application of vacuum. After the complete removal of chloroform, this process led to the formation of a gel-like lipoid consistency inside the RBF surface. The formed gel was then hydrated with buffer (pH 7.4) containing NK at 150 rpm and 46 °C (i.e. above the transition temperature of lipids) for 30 min. The formed suspension of multilamellar liposomes was then kept for a few hours at room temperature. The size of the developed liposomes was further reduced by bath sonication (20 min).[25,26] The composition and schematic preparation method of liposomal formulations are presented in Table 1 and Figure 1A. To create a uniform suspension, a short period of vortexing was also performed. Liposomes were then stored at 4 °C after being centrifuged to remove the nonencapsulated drug. The same approach was utilized to fabricate targeted liposomes, with an additional step of conjugation of the targeting moiety by using carbodiimide chemistry. After the formulation of TPGS-COOH coated liposomes, they were post decorated with targeting ligands such as RGD or AM[27,28] depicted in Figure 1B.

Table 1. Content Formulas of Fabricated Liposomes[a]

Preparations	HSPC (mg)	CHOL (mg)	TPGS (mg)	TPGS-COOH (mg)	NK (mg)	C6/MB Dye (μg)
BL-LS	100	10	20	—	—	—
NK-LS	100	10	20	—	10	—
RGD-NK-LS	100	10	10	10	10	—
AM-NK-LS	100	10	10	10	10	—
C6-LS	100	10	20	—	—	300
C6-RGD-LS	100	10	10	10	—	300
C6-AM-LS	100	10	10	10	—	300
MB-LS	100	10	20	—	—	300
RGD-MB-LS	100	10	10	10	—	300
AM-MB-LS	100	10	10	10	—	300

[a]BL-LS: blank liposomes. NK-LS: nattokinase-loaded liposomes. RGD-NK-LS: RGD decorated nattokinase-loaded targeted liposomes. AM-NK-LS: Abciximab decorated nattokinase-loaded targeted liposomes. C6-LS: C6-loaded liposomes. C6-RGD-LS: RGD decorated C6-loaded targeted liposomes. C6-AM-LS: Abciximab decorated C6-loaded targeted liposomes. MB-LS: MB-loaded liposomes. RGD-MB-LS: RGD decorated MB-loaded targeted liposomes. AM-MB-LS: Abciximab decorated MB-loaded targeted liposomes.

2.2.2. Fabrication of Dye-Loaded Liposomes. The identical approaches described above was used to make dye-loaded targeted liposomes. Briefly, chloroform containing HSPC, CHOL, TPGS, TPGS-COOH, and coumarin-6 (C6) dye/methylene blue (MB) (0.3 mg/mL) was poured into a container. Following the addition of the aqueous phase, the probe sonication was then carried out for 40 s. The temperature was kept at 65 °C throughout the process, as illustrated in Figure 1A, and a rotary evaporator was employed to extract the organic phase. The gel-like lipid mixture was formed that was redispersed with the addition of an aqueous solution to fabricate liposomal vesicles under rotation. Finally, a probe sonicator was used to ultrasonicate the dye-loaded liposomes for 4 min. The resulting liposomes (C6-LS/MB-LS) were then filtered through a 0.22 m filter and examined for their physical features. The targeted dye-loaded formulations were prepared by the above-mentioned procedures by using carbodiimide chemistry.

2.3. Physicochemical Characteristic Evaluations. *2.3.1. Particle Size and Polydispersity Index (PDI) Determination.* A particle size analyzer employing the theory of dynamic scattering of light (S90, Malvern Zetasizer, U.K.) was utilized to measure the particle size and PDI of liposomes. The experiment was performed using a liposomal suspension that had been diluted ten times in Millipore water. At ambient temperature, all the measurements were obtained in triplicate.[29]

2.3.2. Zeta Potential Measurement. Malvern Zetasizer Pro (U.K.) was used to determine the zeta potential of liposomes. The liposomal suspensions were diluted (20×) in the aqueous media, and the charge at the surface of the liposomes, which influences the formulation stability, was determined.[30]

2.3.3. % Encapsulation Efficiency (EE). Liposomes loaded with the drug were disrupted for 3 h at room temperature using bath sonication in methanol. Following the procedure, a 0.22 μ syringe filter was used to filter the residues in the fluid, and a UV spectrophotometer was employed to measure the absorbance at

https://doi.org/10.1021/acs.molpharmaceut.3c00830
Mol. Pharmaceutics 2024, 21, 283−302

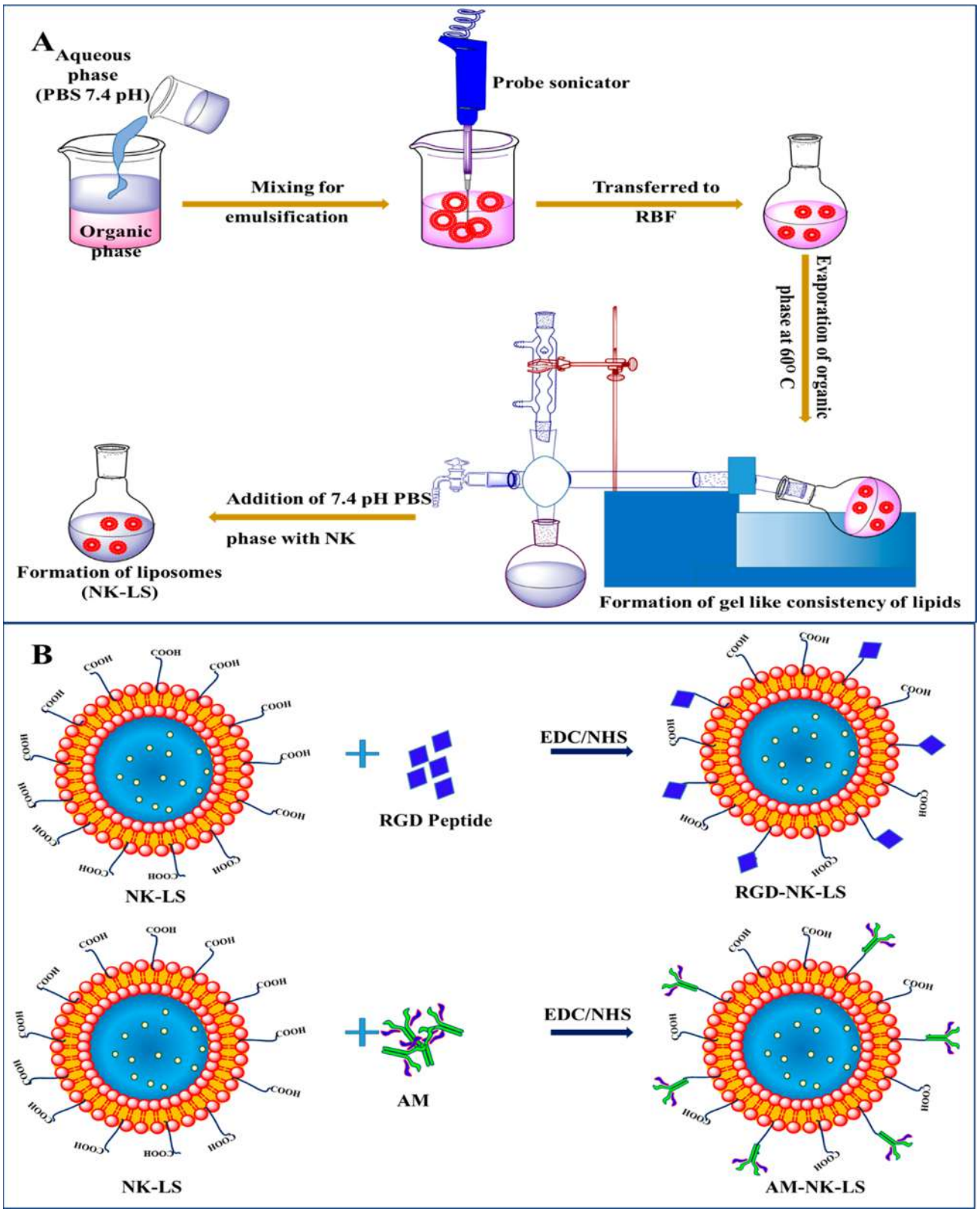

Figure 1. (A) Diagrammatic presentation of the preparation method for NK-LS. (B) Conjugation of RGD or AM on NK-LS by carbodiimide chemistry.

λmax = 660 nm.[31] For the sample analysis, the Lowry method was used for NK detection. The calculation for encapsulation efficiency is shown below:

$$\text{EE}\ (\%) = (\text{Quantity of encapsulated drug}/\text{Quantity of added drug}) \times 100$$

2.3.4. SEM Analysis. The exterior microstructure of NK-LS, RGD-NK-LS, and AM-NK-LS were imaged using an SEM (Nova Nano 450, USA) at 25 °C. To create a uniform thin film, a drop of each liposome sample that had been diluted ten times

https://doi.org/10.1021/acs.molpharmaceut.3c00830
Mol. Pharmaceutics 2024, 21, 283−302

was cast on distinct glass coverslips. Images of liposomes were taken at magnifications of 100 KX and voltage of 20 kV after following overnight drying and carbon coating of the samples.[32]

2.3.5. External Morphology by Transmission Electron Microscopy (TEM). TEM (Tecnai G2 20 TWIN, FEI Company, USA) analysis was used to investigate the shape, size, architecture, and surface morphology of the prepared nontargeted and targeted liposomal preparations. The liposomal suspensions were diluted (20×) and then dispersed uniformly using a bath sonicator for 5 min. Each sample was applied as a single drop to a TEM grid made of copper and allowed to dry overnight in a vacuum before being imaged.[33]

2.3.6. Characterization by Atomic Force Microscopy (AFM). AFM was used to image NK-LS, RGD-NK-LS, and AM-NK-LS (NTEGRA Prima, Netherlands) to analyze the surface features and morphology of these samples. The fabricated liposomal suspensions were diluted (5×) and cast on glass coverslips after being bath sonicated for a few minutes to uniformly disperse the liposomal suspension. The samples were vacuum-dried overnight at room temperature and then subjected to AFM imaging.[34]

2.3.7. Bradford Assay. To create a standard reference curve, bovine serum albumin (BSA) was diluted into aqueous media in a 1 mg/mL concentration. The aliquot from the above solution was taken out (in volumes of 6.25, 12.5, 25, 50, 100, and 200 μL) to produce the necessary dilutions, and an excess of solvent was mixed in the Eppendorf tube to make up the volume up to 1000 μL. Dilutions were made precisely by using micropipettes. The pure AM/RGD dilutions and each targeted liposomal suspensions (similar concentration, diluted 10, 50, and 100 times) were introduced into microwells (triplicate) of a 96-well plate. Each microwell received 10 μL of the sample and Bradford reagent (0.25 mL) in it. Then, the whole setup was kept in the dark for 15 min at room temperature. At last, a microplate reader was used to examine the produced color at a wavelength of 595 nm.[35]

2.3.8. X-ray Diffraction (XRD) Study. The physical properties of the active ingredient (NK) and other constituents of the liposomes were examined in both their purified and nanoforms, to investigate the modifications resulting from the encapsulation in the drug's physical state and crystallinity. The XRD pattern of NK, other excipients, and developed liposomal preparations was obtained using an X-ray diffractometer (Rigaku Miniflex 600, Japan). A 10° min^{-1} scan frequency, X-ray as the source of radiation, 40 kV tube voltage, and 15 mA current, with a step size of 0.02° at a 10−90° 2θ angle, were used to record the diffractograms.[36]

2.3.9. X-ray Photoelectron Spectroscopy (XPS). The surface chemistry of NK-loaded liposomes and targeted liposomes was studied using XPS analysis (K-Alpha, Thermo Fisher Scientific) at a range of 10−800 eV binding energy. A drop of the liposomal suspension was placed on a glass slide (1 cm × 1 cm) and dried under vacuum overnight. The resulting samples were then analyzed using XPS.[37]

2.3.10. Thermogravimetric Analysis (TGA). TGA (Shimadzu, Japan) was used to evaluate the thermal resistance and degradation of NK, HSPC, CHOL, TPGS, and nontargeted liposomes (NK-LS). All of the samples had a weight ranging from 3 to 8 mg, while they were desiccated. TGA measurements of each sample were performed within a temperature range of 25 to 500 °C. In the course of the experiment, the standard N_2 flow rate was maintained, and the 10 °C/min increment in heating rate was utilized.[38]

2.4. *In Vitro* Assessments. *2.4.1. In Vitro Drug Release Study.* The *in vitro* drug release was performed by using the sample separation technique for drug-loaded liposomes. NK-loaded targeted and nontargeted liposomes (1 mg/mL) were placed in phosphate-buffered saline (pH 7.4) in a 1:10 ratio. The system was maintained at 37 ± 0.5 °C with gentle shaking. The samples were withdrawn at different sampling time intervals and were centrifuged to separate both liposomal vesicles and supernatant. The sediment was redispersed with the same volume of medium and again added to the release medium of the ongoing study.[39] The amount of drug released in the supernatant was determined by the Lowry method at λ = 660 nm by using ultraviolet spectroscopy.[40]

2.4.2. Clot Lysis Assay. Antecubital venous blood was withdrawn from healthy human volunteers, who provided their informed consent in accordance with the Institutional Ethical Committee (IEC) recommendations (ECR/526/Inst/UP/2014/RR-20). The whole blood sample was collected and kept in a glass tube in a volume of 1 mL without an anticoagulant. The blood clot formed after a 3-h incubation at 37 °C was weighed and washed with saline to remove other fluidic content. Further, the retracted clots were treated with a saline control and liposomal formulations in a glass tube with incubation at 37 °C. After different time intervals (0, 1, 2, 4, 8, 12 h), the clots were photographed, and at last, they were again weighed to obtain the % clot lysis. Before the weighing, the supernatant content was removed and dried overnight at room temperature, and the % clot lysis was calculated by using the following formula.[41]

$$\text{Percent clot lysis (\% CL)} = \frac{\text{weight of clot before lysis} - \text{weight of clot after lysis}}{\text{weight of clot}} \times 100$$

2.4.3. PT and aPTT Studies. In brief, centrifugation was used to separate plasma from human blood that was stored in citrate-coated tubes. Following this, 200 μL of each of the drug-loaded liposomes was mixed with the same volume of obtained plasma and incubated over 3 min. Later, for PT analysis, 100 μL of plasma was utilized, along with an equal volume of the PT reagent. In contrast, the aPTT test required plasma of about 50 μL together with 0.25 M calcium chloride and the aPTT reagent (Phospholin ES). In this investigation, all reagents were preheated to a temperature of 37 °C. Moreover, in this study, NK was used as a positive control, and pH 7.4 PBS was used as a negative control. Further, a coagulometer (by Diagnostica Stago, France) was used to measure the PT and aPTT.[42]

2.4.4. Platelet Aggregation Study. A platelet aggregation assay was carried out via the turbidimetry technique using a microplate scanner (SpectraMax M5, U.S.). In order to prevent coagulation, citrate-coated containers were used to collect samples of human blood from a healthy adult donor.[43] The platelet-rich plasma (PRP) was then separated using centrifugation at 350*g* for 20 min, and the pellet of the platelets was subsequently obtained using recentrifugation at 1450*g*. The separated platelets were then washed with physiological saline once. A hemocytometer was used to measure the final platelet count, which was then reconstituted to attain a cell count of about 2 × 10^8 cells/mL using platelet-poor plasma (PPP) and denoted as PRP. After this, PRP was incubated with NK, NK-LS, RGD-NK-LS, and AM-NK-LS (1 mg/mL, 100 μL) for 4 min; subsequently, thrombin and fibrinogen were added to initiate aggregation. The percentage of maximum gain in light

https://doi.org/10.1021/acs.molpharmaceut.3c00830
Mol. Pharmaceutics 2024, 21, 283−302

transmission served as the measure for the maximum agglomeration rate (MAR) by using PRP as a control with 100% transmission.[44]

2.4.5. In Vitro Biocompatibility Assessment. 2.4.5.1. Blood Smear. To examine the morphological abnormalities in blood components, a blood smear analysis was carried out. Human blood was withdrawn from healthy volunteers by a venipuncture technique and then collected in tubes coated with sodium citrate. Later, blood was added to saline, NK-LS, RGD-NK-LS, and AM-NK-LS at a similar concentration (1 mg/mL) in an 8:2 ratio. At 4 °C, this mixture were stored for 24 h. Later, a drop of the resulting blood mixture was formed as a smear individually. Wright-Giemsa stain was applied to the developed smear specimens and successively rinsed using pH 7.4 PBS. A bright field microscope was used to examine the prepared smear samples after being air-dried.[42]

2.4.5.2. Assessment of Hemolytic Activity. A hemolysis test was used to evaluate the biocompatibility of the liposomal formulations. Less than 10% of the hemolysis was regarded as safe for human use. Red blood cells (RBCs) were separated from collected human blood by centrifugation at 825× g for 15 min. After removing the supernatant, the RBCs were rinsed three times in PBS as sediment. 100 μL of the prepared RBC suspension (2% v/v in isotonic buffer), along with each liposomal formulations (100 μL, 1 mg/mL of NK), was incubated with PBS as the diluting medium (800 μL). The resultant solution was centrifuged over 5 min at 825*g* after being incubated for 1 h at 37 °C. The obtained supernatant was poured into a 96-well plate in a 200 μL quantity. The RBC solution was diluted to the same concentration (100 μL) with PBS (0.01 M, 7.4 pH) and 1% Triton-X acting as the negative and positive controls, respectively. A microplate scanner was used to measure the absorbance at 540 nm in the absorbance mode. The following equation was employed to determine the percentage of hemolysis.[45]

$$\text{Hemolysis (\%)} = \frac{\text{absorbance of treatment} - \text{absorbance of PBS}}{\text{absorbance of Triton X} - \text{absorbance of PBS}} \times 100$$

2.4.6. In Vitro Clot Targeting Efficiency. 2.4.6.1. IVIS Imaging Analysis. The effectiveness of targeted liposomes to reach activated platelets for site-specific delivery was evaluated *in vitro* by using the Photon Imager Optima, a luminescent imaging tool from the French company Biospace Lab. The C6-loaded liposomal formulations (C6-LS, C6-RGD-LS, and C6-AM-LS) were prepared for this study, and unloaded dye was removed by centrifugation for 20 min at 125*g*. Platelets were separated from human blood, and saline solution was used for their washing. Later, platelets were transferred to glass vials after being resuspended in the initial volume of saline. In order to activate the platelets, 10 μL of thrombin (10 U/mL) and 20 μL of fibrinogen (10 mg/mL) were added to the containers. The containers were simultaneously added to with C6 solution, C6-LS, C6-RGD-LS, and C6-AM-LS, and then the mixture was incubated for an hour. The resulting mixture was then centrifuged for 20 min at a speed of 3250*g* to separate platelets, from the unbound portion of liposomes in the supernatant. The platelets were reconstituted with 7.4 pH PBS and examined using an imaging device. The region of interest (ROI) signals were recorded for each sample and analyzed for their intensities. The amount of C6 was kept equal for each container, and the instrument's specifications were set for excitation and emission wavelengths of 575 and 550 nm.[46,47]

2.4.6.2. Image-J Analysis of Confocal Microscopic Images. The activated platelets (in cell concentration 3×10^7) were incubated with 100 μL of C6-loaded liposomes (C6-LS, C6-RGD-LS, and C6-AM-LS) for an hour. Then, the cells were fixed using a 4% v/v paraformaldehyde solution. pH 7.4 PBS was used to wash the cells three times to get rid of extra noninteracted liposomes. The *in vitro* efficiency of clot targeting was assessed by using ImageJ software to quantify the percentage of green channels in the resulting CLSM images of interacted platelets. ImageJ was used to convert the pictures to white and black binary pictures, and the dark areas were quantified to represent the intensity of the green channel in CLSM images, which measures the affinities of C6-LS, C6-RGD-LS, and C6-AM-LS toward activated platelets.[48,49]

2.4.7. In Vitro Fibrinolysis by Confocal Microscopy. The 1 mg/mL solution of purified human fibrinogen was prepared in Tris-HCl (50 mM) and NaCl (140 mM) based buffer (pH 7.4). A fluorescently labeled clot was formed by using Alexa Fluor 488-conjugated fibrinogen (10 μL) and human fibrinogen (90 μL) (ratio of 1:9), which was followed by the addition of $CaCl_2$ (2 mM) and thrombin (1 U/mL) to initiate fibrin polymerization. The above mixture was transferred onto fabricated glass slides (depth: 350 μm) as mentioned and incubated for 1 h at 37 °C to allow thrombus formation.[50] A 20 μL aliquot of NK, NK-LS, RGD-NK-LS, and AM-NK-LS solutions (100 μg/mL) was added to fabricated glass slides containing fluorescent clots, respectively. After, a 10-min incubation of the drug or liposomes, the slide was covered with a coverslip. The extent of fibrinolysis was observed under the confocal laser scanning microscope (ZEISS LSM 900, Bangalore, India) equipped with a plan apochromat 1.4 NA oil immersion objective (63×), 488 nm argon ion laser, and LSM acquisition software.

2.4.8. In Vitro Visualization of the Interaction of Nanomedicine with Activated Platelets by Flow Cytometry. Platelets were isolated from freshly collected human blood by using differential centrifugation as reported earlier[51] in the presence of prostaglandin-1 (PGE-1,1 μM) and EDTA (2 mM) to avoid activation. In brief, blood was collected in a sodium citrate tube and centrifuged to get platelet-rich plasma which was followed by washing in Buffer A. Further, pelleted cells were centrifuged and resuspended in Buffer B at a final concentration of 2×10^8/100 μL. The platelets were fluorescently labeled using CD41a antibody and further incubated with C6-loaded liposomes (C6-LS, C6-RGD-LS, and C6-AM-LS) to acquire the potential interaction using a flow cytometer tool. All the samples were incubated in the dark at room temperature for 30 min and subjected to flow cytometer analysis. The fluorescent data were collected by 4-quadrant logarithmic amplification. The FL-1 Channel mean was considered to plot a comparative intensities graph.[52]

2.4.9. Stability Assessment. 2.4.9.1. Serum Stability. The stability of NK-LS in fetal bovine serum (10% v/v, FBS) was performed using size distribution examination. 10% v/v FBS was added to the liposomal preparation, which was then incubated in the dark for 3 days. The particle size and PDI of the preparations were then measured prior to and post process.[53]

2.4.9.2. Stability on Storage. The particle size of the prepared liposomal formulations was analyzed after being diluted ten times in aqueous medium. The samples were kept at 4−8 °C for 3 months. The size of the liposomal preparations was evaluated after the specified period (3 months) to assess stability.[21]

https://doi.org/10.1021/acs.molpharmaceut.3c00830
Mol. Pharmaceutics 2024, 21, 283−302

Table 2. Physicochemical Parameters of Liposomal Formulations

Liposome type	Particle size (nm) (Mean ± SD[a])	PDI (Mean ± SD[a])	Zeta potential (mV) (Mean ± SD[a])	% EE (Mean ± SD[a])	C6 or MB% EE (Mean ± SD[a])
NK-LS	162.8 ± 4.4	0.178 ± 0.010	−06.65 ± 0.58	73.20 ± 1.76	—
RGD-NK-LS	173.4 ± 5.6	0.261 ± 0.085	−08.96 ± 0.96	69.96 ± 2.46	—
AM-NK-LS	177.7 ± 4.9	0.275 ± 0.054	−09.24 ± 1.59	69.76 ± 1.42	—
C6-LS	165.8 ± 3.5	0.178 ± 0.019	−12.08 ± 0.30	—	75.10 ± 3.19
C6-RGD-LS	175.0 ± 6.3	0.200 ± 0.018	−13.99 ± 1.62	—	71.20 ± 1.76
C6-AM-LS	180.2 ± 6.9	0.223 ± 0.017	−15.54 ± 1.66	—	71.53 ± 1.79
MB-LS	166.4 ± 4.3	0.198 ± 0.025	−06.63 ± 0.15	—	72.19 ± 2.15
RGD-MB-LS	176.9 ± 3.4	0.272 ± 0.076	−10.81 ± 0.53	—	70.06 ± 2.52
AM-MB-LS	178.9 ± 3.3	0.235 ± 0.025	−09.95 ± 0.07	—	68.66 ± 1.69

[a]n = 3; SD: Standard deviation.

2.5. *In Vivo* Assessment of Targeted Nanomedicines. All the *in vivo* animal experiments were approved by the Institutional Animal Ethics Committee (IAEC) of Indian Institute of Technology, Banaras Hindu University, Varanasi (IIT(BHU)/IAEC/2022/051).

2.5.1. In Vivo Bleeding Time Analysis. Animal bleeding times are measured primarily to assess the hemorrhagic properties of antithrombotic medications. Swiss albino mice (male) were selected (age of 5−7 weeks, weighing around 20 ± 2 g) and randomly categorized in 5 different groups (n = 3) for a tail bleeding study. A 0.5 mg/kg dosage of NK and various liposomal formulations were given intravenously through the tail vein, and an equal volume of saline was administered as the negative control. The NK concentration was kept equal for both nontargeted and targeted liposomes. Later, anesthesia was given to mice before being placed on a platform with the heat control (37 °C) in the supine posture. Following the end of the 1-h latent phase, the tail of the mice was cut off at 1 cm away from the tip using a surgical blade. The tail was immediately immersed in saline (50 mL) after transection. Bleeding time was defined as the point of time at which the bleeding ceased. The most extended time noted was not more than 400 s.[53,54]

2.5.2. In Vivo Clotting Time Analysis. The previously reported method was to measure the blood clotting time in Swiss albino mice. NK and liposomal formulations (i.e., NK, NK-LS, RGD-NK-LS, and AM-NK-LS) were administered through the tail vein at a dose of 500 μg/kg. Additionally, saline was used in equal volumes to the other formulations as a control. After an hour of the i.v. administration, the tip of the tail was intersected by using a surgical blade, and a micro hematocrit capillary tubes was used to collect about 25 μL of blood. The capillary was tilted at an angle of 60° in both the up and down directions to allow blood to flow through it. When blood contacted, the capillary tube stopwatch was started simultaneously. As soon as the blood flow ceased inside the capillary tube with the horizontal plane, the stopwatch was stopped, and the blood clotting time was noted and reported.[55]

2.5.3. In Vivo Thrombolysis Assessment by a Doppler Flow Meter. SD rats were housed in cages at constant room temperature and given access to food or water. Isoflurane was used at a dose of 3% in oxygen through an inhalation route to anesthetize the rats. In order to avoid hypothermia, the animals were put on a heat-controllable surgical platform. After careful removal of hair, the carotid artery was exposed via median incision on the ventral neck region, which was followed by adequate cleansing to isolate the common carotid artery from adjacent tissues. The routine blood flow of the animals was recorded using a Blood Flow Meter (Transonic, model T106) by placing the pulsed flow probe (1 PRB; PR-series, Transonic system) on the carotid artery. Afterward, a Whatmann filter paper soaked with $FeCl_3$ (20% w/v) was topically applied to the already exposed carotid artery for 5 min to induce thrombus formation. A small piece of parafilm was kept under the exposed carotid artery in order to prevent $FeCl_3$ contact and damage to other tissues. The cessation of blood flow (the time of occlusion after applying $FeCl_3$) was recorded using a flow probe, and data were analyzed by a PC-driven PowerLab data acquisition system employing LabChart Pro software (AD Instruments). The NK and liposomal formulations (i.e., NK, NK-LS, RGD-NK-LS, and AM-NK-LS) were administered through the tail vein at doses of 1 mg/kg each for 10 min following $FeCl_3$ application, when blood flow showed maximum decline. The extent of clot lysis was measured from the magnitude of restoration of blood flow.[56,57]

2.5.4. In Vivo Thrombolysis by Ultrasound Imaging. Clot lysis efficacy of fabricated liposomes was analyzed using an Ultrasound imaging tool (Vevo LAZR-X; Fuji Film Visual Sonics, Inc.), which provides high-resolution and real-time imaging data of the scanned area. Rats were randomly categorized into five groups (n = 3). The right carotid artery was exposed, as described above. Routine blood flow was measured by employing high-frequency ultrasound transducers in Pulsed-wave Doppler mode using Vevo LAZR-X. Thrombus generation was induced with $FeCl_3$ (10% w/v) leading to a decline in blood flow velocity. Prepared liposomes were injected into rats intravenously, as stated above. The regain in blood flow was recorded and analyzed with Vevo LAB software.

2.5.5. In Vivo Targeting Capability by Photoacoustic Imaging (PAI). The targeting efficacy of fabricated liposomes toward thrombus was analyzed by photoacoustic imaging in Live unmixing mode, which uses computational techniques to separate and identify various components within the signal or image. Liposomes were labeled with methylene blue and intravenously injected into the rat, followed by induction of thrombus formation with $FeCl_3$. Whenever MB-LS is exposed to a laser, the dye undergoes a photochemical reaction to absorb photons. This leads to the generation of a photoacoustic signal, which is further detected by the ultrasonic transducer. An accumulation of labeled liposomes at the thrombus site was underscored from an enhanced PA signal at the scanned area, after 15 min of administration, which indicated efficient *in vivo* thrombus targeting.[58,59]

2.5.6. Histopathological Assessment. Histopathological examination was carried out to determine the adverse effects and mortality that follow treatment using liposomal preparation. The Sprague−Dawley rats (n = 3) with a mixed gender

https://doi.org/10.1021/acs.molpharmaceut.3c00830
Mol. Pharmaceutics 2024, 21, 283−302

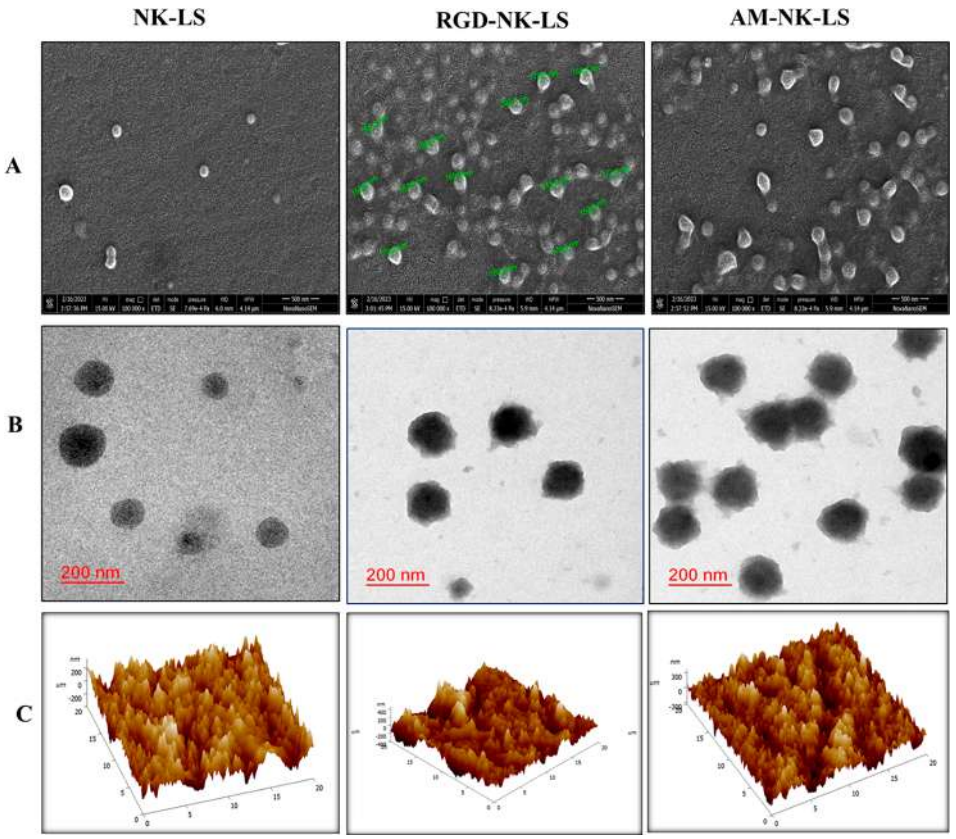

Figure 2. A) SEM, B) TEM, and C) 3D AFM images of nontargeted and targeted liposomes.

population weighing about 200 ± 20 g had received the liposomal formulations through intravenous bolus at a dose of 1 mg/kg. Following administration, 14 days were spent monitoring to check for acute and chronic toxicity. The formulation was deemed safe or well-tolerated based on observation.[60,61]

3. RESULTS AND DISCUSSION

3.1. Physicochemical Characteristic Evaluations.

3.1.1. Evaluation of Particle Size, PDI, and Zeta Potential. The mean of the particle size of NK-LS, RGD-NK-LS, and AM-NK-LS was determined by a Zetasizer and found to be 162.8 ± 4.4, 173.4 ± 5.6, and 177.7 ± 4.9 nm, while for C6-loaded liposomes, the size was recorded as 165.8 ± 3.5, 175.0 ± 6.3, and 180.2 ± 6.9 nm in the case of C6-LS, C6-RGD-LS, and C6-AM-LS, respectively. Additionally, the particle sizes of MB-LS, RGD-MB-LS, and AM-MB-LS were noted as 166.4 ± 4.3, 176.9 ± 3.2, and 178.9 ± 3.3, respectively. The PDI of all the liposomal preparations was less than 0.3 when presented as Mean ± SD. Moreover, the zeta potential of the liposomal preparations was −06.65 ± 0.58, −08.96 ± 0.96, and −09.24 ± 1.59 mV for NK-LS, RGD-NK-LS, and AM-NK-LS, respectively. The C6-loaded liposomes showed zeta potential values around −12.08 ± 0.30, −13.99 ± 1.62, and −15.54 ± 1.66 mV for C6-LS, C6-RGD-LS, and C6-AM-LS, respectively. All related data are presented in Table 2.

3.1.2. Encapsulation Efficiency. According to the literature, the extent of drug loading was estimated by % encapsulation efficiency (% EE) which is defined as the proportion of the drug incorporated within the liposomal vesicles out of the total amount initially added. The % EE of nontargeted liposomes was calculated and found to be 73.20 ± 1.76%, while in the case of RGD-NK-LS and AM-NK-LS, the % EE was estimated as 69.96 ± 2.46% and 69.76 ± 1.42%, respectively. Moreover, the % EE of the C6-loaded formulations was found to be 75.10 ± 3.19, 71.20. ± 1.76, and 71.53 ± 1.79% for C6-LS, C6-RGD-LS, and C6-AM-LS, respectively.

3.1.3. SEM and TEM Analyses. The SEM and TEM images of NK-LS, RGD-NK-LS, and AM-NK-LS were obtained, as depicted in Figures 2A and 2B. The liposomes (NK-LS, RGD-NK-LS, AM-NK-LS) were spherical in shape suggested by the morphological investigations of the pictures that all are without any pin and holes. Moreover, the average size of all of the preparations was under 200 nm. In addition, in the TEM images, the surface of the targeted liposomes revealed the successful coating of targeting peptides.

3.1.4. AFM Analysis. Figure 2C shows the AFM 3D micrographs of nontargeted and GPIIb/IIIa-targeted liposomes. The image presented the surface property of liposomes with a smooth exterior without any pin and hole imperfections. These images further proved that the prepared liposomes were spherical in shape, with uniform distribution of particle size ranging under 200 nm.

3.1.5. Bradford Assay. The Bradford test was used to estimate the protein content in samples. The degree of conjugation of AM and RGD at the surface of targeted liposomes was estimated at around 70.20 ± 3.14% and 68.86 ± 3.01% for RGD-NK-LS and AM-NK-LS, respectively. Here, % denotes the proportion of the initial amount of added antibody or peptide that has been associated with surface COOH function of the liposomes.

3.1.6. XRD Analysis. The XRD spectrum overlay shown in Figure 3A represents the distinct peaks of drug (NK), vesicle components (HSPC, CHOL, TPGS), and liposomal formula-

https://doi.org/10.1021/acs.molpharmaceut.3c00830
Mol. Pharmaceutics 2024, 21, 283−302

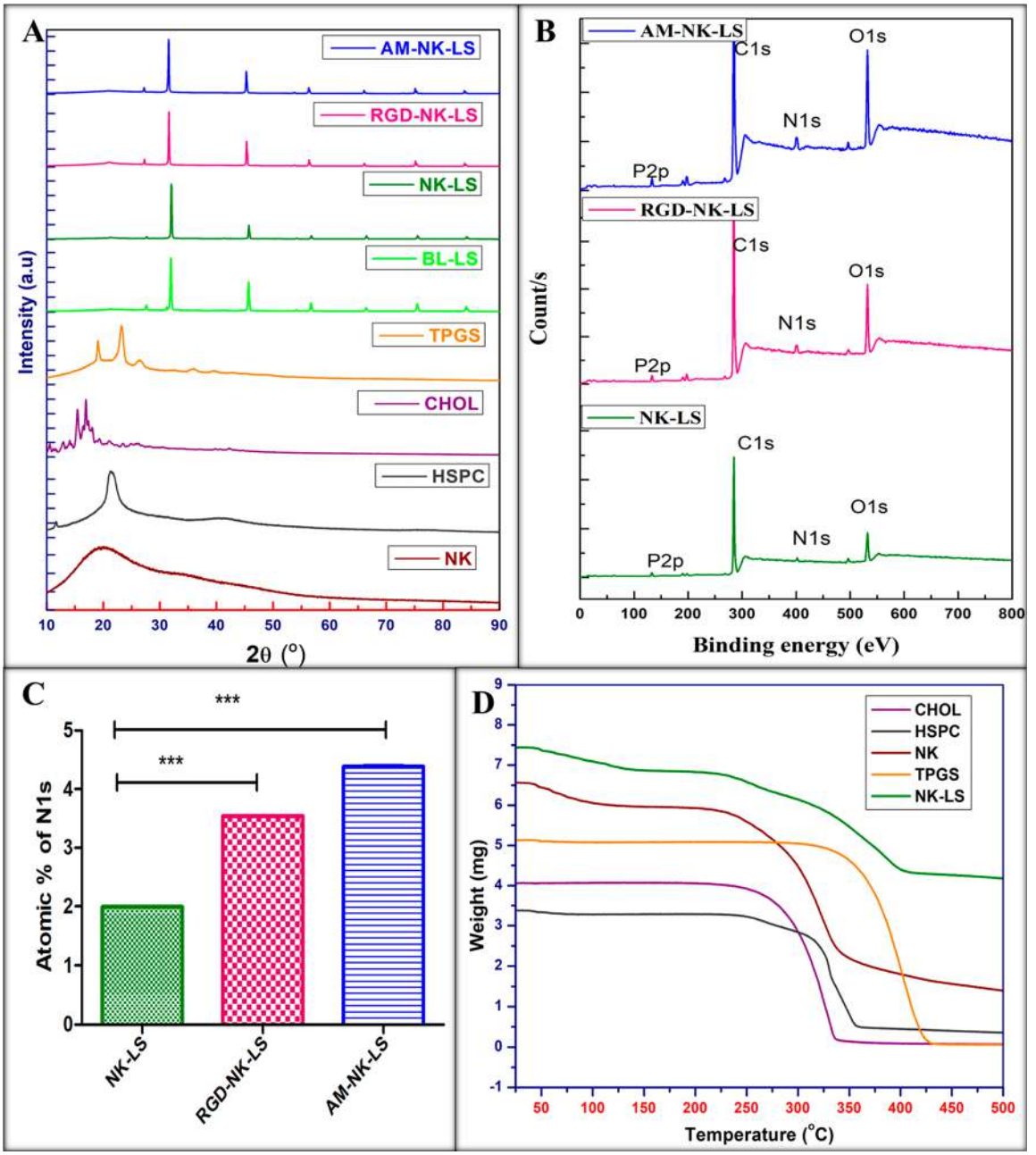

Figure 3. A) XRD spectra overlay of NK, HSPC, CHOL, TPGS, nontargeted, and targeted liposomes. B) XPS survey of NK-LS, RGD-NK-LS, and AM-NK-LS. C) Bar graph representing atomic % of N 1s in the XPS spectra. D) TGA overlay of the components of liposomes and NK-LS.

tions at the 2θ angle. NK showed a broad peak in the range of 10°−30° angles, whereas HSPC exhibited a broad peak in the range of 20°−25° angles. However, CHOL and TPGS showed a few sharp peaks at the angles of 12.83°, 14.13°, 15.42°, 16.91° and 19.14°, 23.28°, 26.46°, respectively. Furthermore, all the liposomal formulations showed the characteristic sharp peaks at the 2θ angles of 31.85°, 45.75°, 56.35°, 66.31°, 75.56°, and 84.30° representing their physicochemical properties.

3.1.7. Surface Chemistry. XPS spectral analysis was utilized to investigate the surface chemistry of NK-LS (nontargeted) as compared to targeted liposomes (RGD-NK-LS and AM-NK-LS). Figure 3B represents the characteristic peaks of different constituents such as P, C, N, and O that are present in the liposomal constitution illustrated in the XPS spectra. The peaks obtained at different binding energies like 129−138, 280−291, 395−406, and 528−539 signify the presence of phosphorus (P 2p), carbon (C 1s), nitrogen (N 1s), and oxygen (O 1s) at the surface of liposomes. The % amount of C 1s, N 1s, and O 1s was 86.41%, 1.98%, and 11.61% in the case of NK-LS, whereas the % amount was changed in the case of targeted liposomes to 83.63%, 3.54%, and 12.82% in RGD-NK-LS and 81.95%, 4.33%, and 13.72% in AM-NK-LS, respectively. The comparative bar graph of the nitrogen content is presented in Figure 3C.

3.1.8. Thermogravimetric Analysis (TGA). Figure 3C illustrates the TGA graphs of NK, CHOL, TPGS, HSPC, and NK-LS in the temperature range 25−500 °C. The initial decline in sample mass represents the elimination of moisture content due to the evaporation process, and the secondary decline corresponds to the product degradation over the range of differential temperatures. In the case of NK, an initial weight loss

https://doi.org/10.1021/acs.molpharmaceut.3c00830
Mol. Pharmaceutics 2024, 21, 283−302

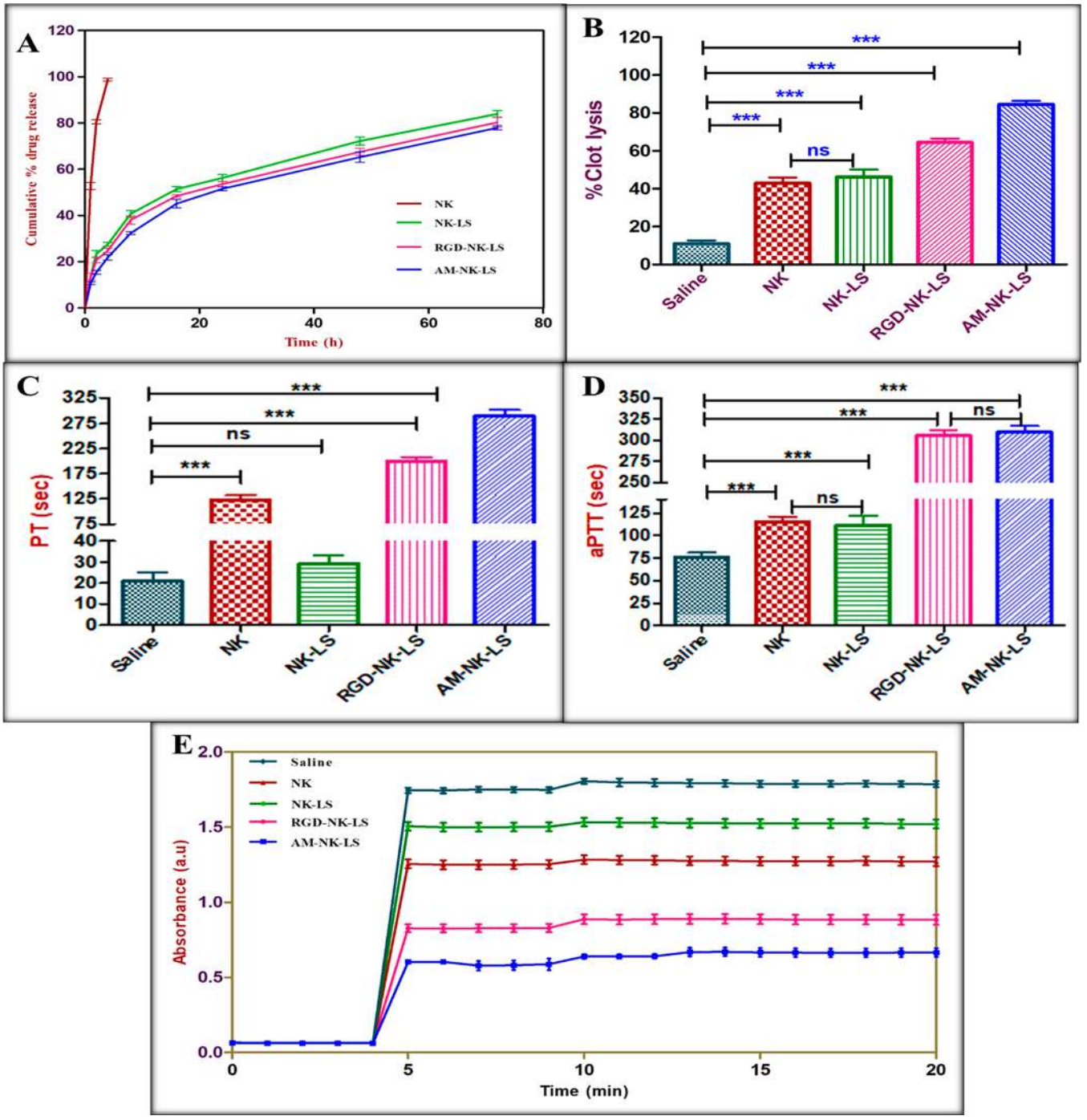

Figure 4. A) CPR vs time plot of nontargeted and targeted nanoformulations. Bar graph showing B) % clot lysis, C) PT values, and D) aPTT values. E) Line graph showing platelet aggregation in terms of the absorbance of saline, NK, NK-LS, RGD-NK-LS, and AM-NK-LS. All figures are representative of three independent experiments, and data are shown as a Mean ± SD (n = 3), where ns ($p \geq 0.05$), ***$p < 0.001$, **$p < 0.01$, and *$p < 0.05$.

of 8.71% was observed due to the removal of moisture content in the temperature of 40−140 °C. However, the gradual loss of mass (63.31%) was noted as a second decline phase between 220 and 345 °C, and the losing of mass continues to 500 °C with a loss of 78.44% of the total content. Other ingredients of the liposomal constitution such as CHOL (221.82 to 338.29 °C), HSPC (249.55 to 359.93 °C), and TPGS (315.56 to 431.05 °C) showed a sudden loss in mass of 97.25%, 85.84%, and 98.38%, respectively, in the short temperature range in their initial decline phase. Moreover, for NK-LS, the primary decline phase in the TGA plot was observed due to the moisture removal at the range of 40−140 °C showing an 8.07% elimination of total mass. Additionally, the subsequent decline in mass was observed at 200−400 °C in a progressive manner showing a 44.54% loss of total mass at 500 °C.

3.2. *In Vitro* Studies. *3.2.1. In Vitro Drug Release Study.* Figure 4A illustrates the cumulative % drug release (CPR) rates of NK from nontargeted and targeted formulations at systemic pH 7.4. The % release was estimated after 72 h of study, and it showed 83.96 ± 2.05, 80.3 ± 2.94, and 77.96 ± 1.24% CPR; however, at 24 h%, CPR was 56.25 ± 2.16, 53.58 ± 1.69, and

https://doi.org/10.1021/acs.molpharmaceut.3c00830
Mol. Pharmaceutics 2024, 21, 283−302

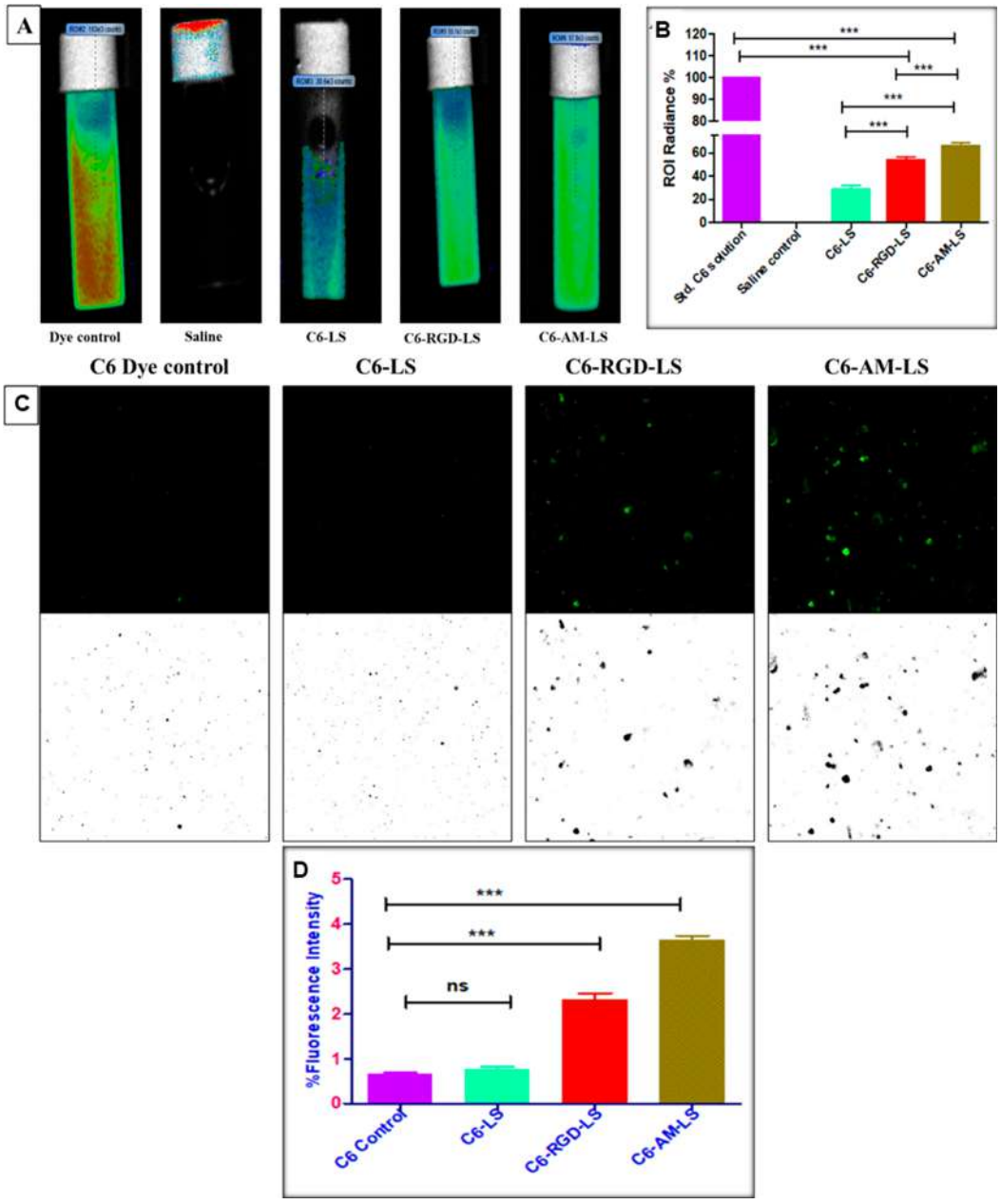

Figure 5. A) Bioluminescence images representing the platelet interaction potential of C6-LS, C6-RGD-LS, and C6-AM-LS in comparison with the C6 dye control. B) Bar graph showing comparative % ROI radiance. C) CLSM fluorescent and corresponding binary images of platelet binding affinity when treated with C6 dye, C6-LS, C6-RGD-LS, and C6-AM-LS. D) Bar graph presenting relative % fluorescence intensity. All the bar graphs are representative of three individual experiments with Mean ± SD (n = 3), where ns ($p \geq 0.05$), ***$p < 0.001$, **$p < 0.01$, and *$p < 0.05$.

51.58 ± 1.24% for NK-LS, RGD-NK-LS, and AM-NK-LS, respectively.

3.2..2. Clot Lysis Assay. The blood clot lysis study was performed for fabricated liposomal formulations in comparison with pure drug (NK) to acquire fibrinolytic potency. The images were taken at different time intervals (0, 1, 2, 4, 8, 12 h) to get insight into the lysis process, as presented in Figure S1. The negative control (saline) was used as a standard to calculate % clot lysis. The % clot lysis was observed at 11.08 ± 2.28, 42.93 ± 4.20, 46.26 ± 5.45, 64.40 ± 3.05, and 84.50 ± 2.60% for saline, NK, NK-LS, RGD-NK-LS, and AM-NK-LS, respectively, as shown in Figure 4B.

3.2.3. PT and aPTT Studies. One of the essential investigations to look into a drug's antithrombotic efficacy is coagulation time evaluation. In this investigation, human plasma was incubated with each liposomal formulation for 3 min before the *in vitro* PT and aPTT were measured. Figures 4C and 4D demonstrate that the PT and aPTT values for the control (saline) group were 20.90 ± 3.48 and 76.03 ± 4.01 s, respectively. The PT values were estimated as 123.63 ± 6.89, 29.36 ± 3.13, 199.9 ± 7.02, and 289.96 ± 10.20 s for NK, NK-LS, RGD-NK-LS, and AM-NK-LS, respectively. Additionally, the aPTT values for NK, NK-LS, RGD-NK-LS, and AM-NK-LS were found to be 114.75 ± 5.30, 111.30 ± 8.61, 305.83 ± 5.12, and 309.96 ± 5.57 s, respectively.

3.2.4. Platelet Aggregation Study. Platelet aggregation occurs when fibrinogen's binding to GPIIb/IIIa receptors initiates primary hemostasis. Resting platelets are gradually

https://doi.org/10.1021/acs.molpharmaceut.3c00830
Mol. Pharmaceutics 2024, 21, 283−302

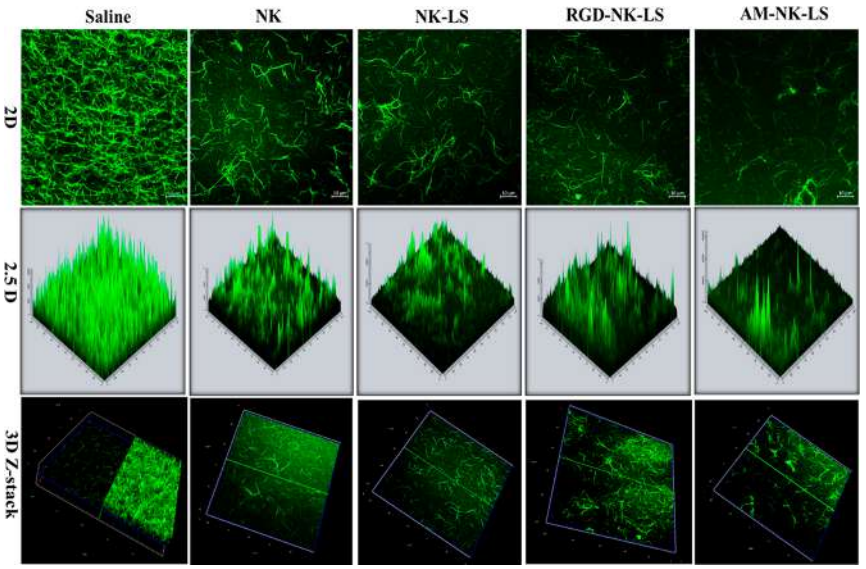

Figure 6. CLSM images represent the comparative fibrinolysis induced by NK, NK-LS, RGD-NK-LS, and AM-NK-LS.

activated and bind with one another to create an aggregate as a result of the hemostasis process. After adding the fibrinogen, saline, NK, and NK-LS line graphs displayed maximum absorbance, but as shown in Figure 4E, the targeted liposomes i.e., RGD-NK-LS and AM-NK-LS showed much less absorbance than the control group.

3.2.5. In Vitro Biocompatibility Assessment. 3.2.5.1. Blood Smear. Figure S2A shows the images of the blood smear obtained after the incubation with saline, NK-LS, RGD-NK-LS, and AM-NK-LS. All of the images were taken at a 10× magnification with the help of a bright-field microscope. The visual analysis of the images presented no morphological changes or rupture of blood cells after the treatment.

3.2.5.2. Hemolytic Assay. The safety and biocompatibility of the nontargeted and targeted liposomes in human blood were examined. The % hemolysis was noted as 1.67 ± 0.48, 1.84 ± 0.74, 1.47 ± 0.64, and 1.62 ± 0.20% for NK, NK-LS, RGD-NK-LS, and AM-NK-LS, respectively, by considering that the distilled water caused 100% lysis and served as a positive control. Saline showed no hemolysis and was used here as a negative control. The findings in Figure S2B show that no liposomal formulation was hemolytic to human blood.

3.2.6. In Vitro Clot Targeting Efficiency. 3.2.6.1. IVIS Imaging Analysis. The ability of nontargeted and targeted liposomes to interact with activated platelets was determined by *in vitro* imaging with C6 loading in liposomes as a contrast agent. The platelets were dispersed in phosphate buffer saline after the incubation with C6 dye control, saline control, C6-LS, C6-RGD-LS, and C6-AM-LS. The bioluminescent radiance was recorded in terms of ROI values ($p/s/cm^2/Sr$) with the help of photon imager optima. The % ROI radiance was calculated in comparison with the standard reference dye control and noted as 28.70 ± 3.02, 53.86 ± 2.26, and 66.04 ± 2.41 for C6-LS, C6-RGD-LS, and C6-AM-LS, respectively, as shown in Figures 5A and 5B.

3.2.6.2. Image-J Analysis of Confocal Microscopic Images. The platelet binding affinity of C6-LS and targeted liposomes (C6-RGD-LS and C6-AM-LS) was determined by the ImageJ analysis of CLSM images. The green channel intensity of the obtained images after the treatment of platelets with dye-loaded liposomes was estimated quantitatively. The obtained images were converted into binary white and black micrographs after being processed. Further, these images were quantified for the dark zone representing the platelet binding affinity. The fluorescent intensity of treated platelets in the green channel was found to be 0.663 ± 0.037, 0.764 ± 0.088, 2.329 ± 0.187, and 3.653 ± 0.126% for the C6 dye control, C6-LS, C6-RGD-LS, and C6-AM-LS, respectively. The fluorescent images and % fluorescent intensity bar graph are presented in Figures 5C and 5D.

3.2.7. In Vitro Fibrinolysis by Confocal Microscopy. The extent of fibrin clot lysis was observed by CLSM at an excitation wavelength of 493 nm and emission wavelength of 517 nm. The Multialkali-PMT detector was used to analyze the samples. The high fluorescence intensity was observed in the control group due to densely packed intact fibrin polymers; however, in the case of drug/liposomes treated samples, due to the clot lysis effect, we observed detachment of strands or a loosely packed fibrin structure represented in Figure 6. The targeted liposomes showed more lysis than NK and nontargeted formulations. The Z-stack images were also observed to assess the lytic efficacy, the control group had z scale or thickness of around 35 μm, and other test groups i.e. NK, NK-LS, RGD-NK-LS, and AM-NK-LS showed a thickness of around 3.99, 2.47, 1.71, and 1.52 μm, respectively, after lysis of fibrinogen in fabricated slides.

3.2.8. In Vitro Visualization of the Interaction of Nanomedicine with Platelets by Flow Cytometry. The flow cytometry was performed to study the binding efficiency of targeted nanomedicines with platelets under *in vitro* conditions (platelets with or without targeted nanomedicines). The flow cytometry mainly estimates the potential affinity of formulated liposomes toward activated platelets. The UR means of FL-1 channels was recorded, and it was found to be around 12, 122, 132.6, and 137% for resting platelets, C6-LS, C6-RGD-LS, and C6-AM-LS. A higher shift in intensities was noted for targeted liposomes than for nontargeted liposomes. The flow cytometry data are presented in Figure S3.

3.2.9. Stability Assessment. 3.2.9.1. Serum Stability. By evaluating the spectra of size distribution of NK-LS prior to and after incubation in 10% v/v FBS, which was acquired by a dynamic light scattering particle size detector, the serum stability was determined. In the investigation, the NK-LS size

https://doi.org/10.1021/acs.molpharmaceut.3c00830
Mol. Pharmaceutics 2024, 21, 283−302

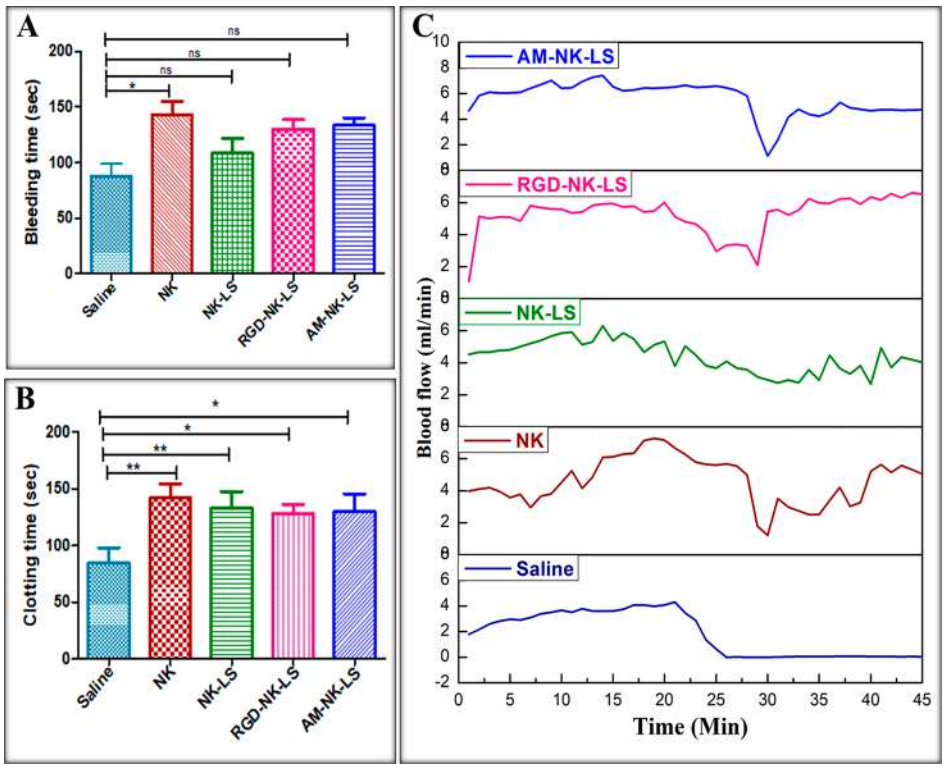

Figure 7. Bar graph showing A) bleeding time and B) clotting time of NK, NK-LS, RGD-NK-LS, and AM-NK-LS in comparison with the saline control. C) Line graph representing blood flow in rat carotid artery after and before clot lysis, when administered with drug, nontargeted, and targeted liposomal formulations. These data are indicative of three different sets of experiments, represented as Mean ± SD ($n = 3$), where ns ($p \geq 0.05$), ***$p < 0.001$, **$p < 0.01$, and *$p < 0.05$.

distribution curve showed a single broad peak between 40 and 500 nm. FBS, on the other hand, had two partial peaks: the first at 45−100 nm and the second at 100−900 nm. After incubation, a doublet of peak around the 35−550 nm range was observed without any notable segregation of the previous size. The line graph in Figure S4 represents the outcomes of the study.

3.2.9.2. Stability of Storage. The stability assessment was carried out to investigate the size and structural integrity of the fabricated liposomal formulations upon storage. The outcome suggests, after storage, that the size and PDI of NK-LS, RGD-NK-LS, and AM-NK-LS had not changed significantly. Table S1 represents the size and PDI values prior to and post storage.

3.3. *In Vivo* Assessment of Targeted Nanomedicines.

3.3.1. In Vivo Bleeding Time Analysis. A tail bleeding study was widely utilized to identify hemorrhagic attributes of antithrombotic medications. The mice were used to record bleeding time following the intravenous injection of antithrombotic medications and the cutting off of the tail tip after 1 h of administration. The bleeding times for saline, NK, NK-LS, RGD-NK-LS, and AM-NK-LS were recorded as 87.66 ± 16.04, 143.33 ± 16.99, 108.33 ± 19.39, 130.33 ± 11.89, and 133.66 ± 9.46 s, respectively. Figure 7A shows the bar graph of the relative bleeding time of various liposomal preparations.

3.3.2. In Vivo Clotting Time Analysis. The amount of time needed to produce thrombin in order to cease bleeding is known as the clotting time. The capillary tube method was used to perform this study on mice, and clotting time was recorded until 300 s using a stopwatch. Saline, NK, NK-LS, RGD-NK-LS, and AM-NK-LS showed a clotting time of around 84.66 ± 10.873, 141.66 ± 10.27, 132.66 ± 12.11, 128.33 ± 6.23, and 129.66 ± 12.97 s, respectively. Figure 7B illustrates a bar graph with a comparative analysis of the clotting times.

3.3.3. In Vivo Thrombolysis Assessment by a Doppler Flow Meter. The clot lysis efficacy of nanoformulations was investigated *in vivo* in a rat (carotid) thrombosis model by a Doppler blood flow meter. The decline or obstruction in blood flow due to the growth of thrombus was observed when Whatmann filter paper soaked with $FeCl_3$ (20% w/v) was applied to the carotid artery for 5 min. The blood flow was partially or fully restored upon the intravenous injection of drug or liposomes and denoted in terms of % regain in blood flow. The percent regain in blood flow was calculated for saline, NK, NK-LS, RGD-NK-LS, and AM-NK-LS and found to be 2.12 ± 0.76, 49.02 ± 2.90, 50.24 ± 4.04, 86.36 ± 4.67, and 66.24 ± 2.68%, respectively. The plots of *in vivo* thrombolysis are shown in Figure 7C, and a comparative bar diagram representing the % regain in blood flow is presented in Figure S5.

3.3.4. In Vivo Thrombolysis by Ultrasound Imaging. Thrombus lytic efficacy of the prepared liposomes was analyzed by real-time Pulsed-wave Doppler mode on the Vevo LAZR-X imaging platform. The physiological blood flow velocity or Doppler spectrum was recorded by applying a Doppler gate of 0.5 mm at the center of the carotid artery. The rats were intravenously injected with saline, NK, NK-LS, RGD-NK-LS, and AM-NK-LS, respectively, when the blood flow declined by thrombus formation in the artery. After 30 min of injection, the animals were again subjected to high-resolution ultrasound imaging, and Doppler spectra were recorded, as shown in Figure 8. The percent of thrombolysis in terms of regain of blood flow velocity after application of $FeCl_3$ with subsequent treatment with saline, NK, NK-LS, RGD-NK-LS and AM-NK-LS was

https://doi.org/10.1021/acs.molpharmaceut.3c00830
Mol. Pharmaceutics 2024, 21, 283−302

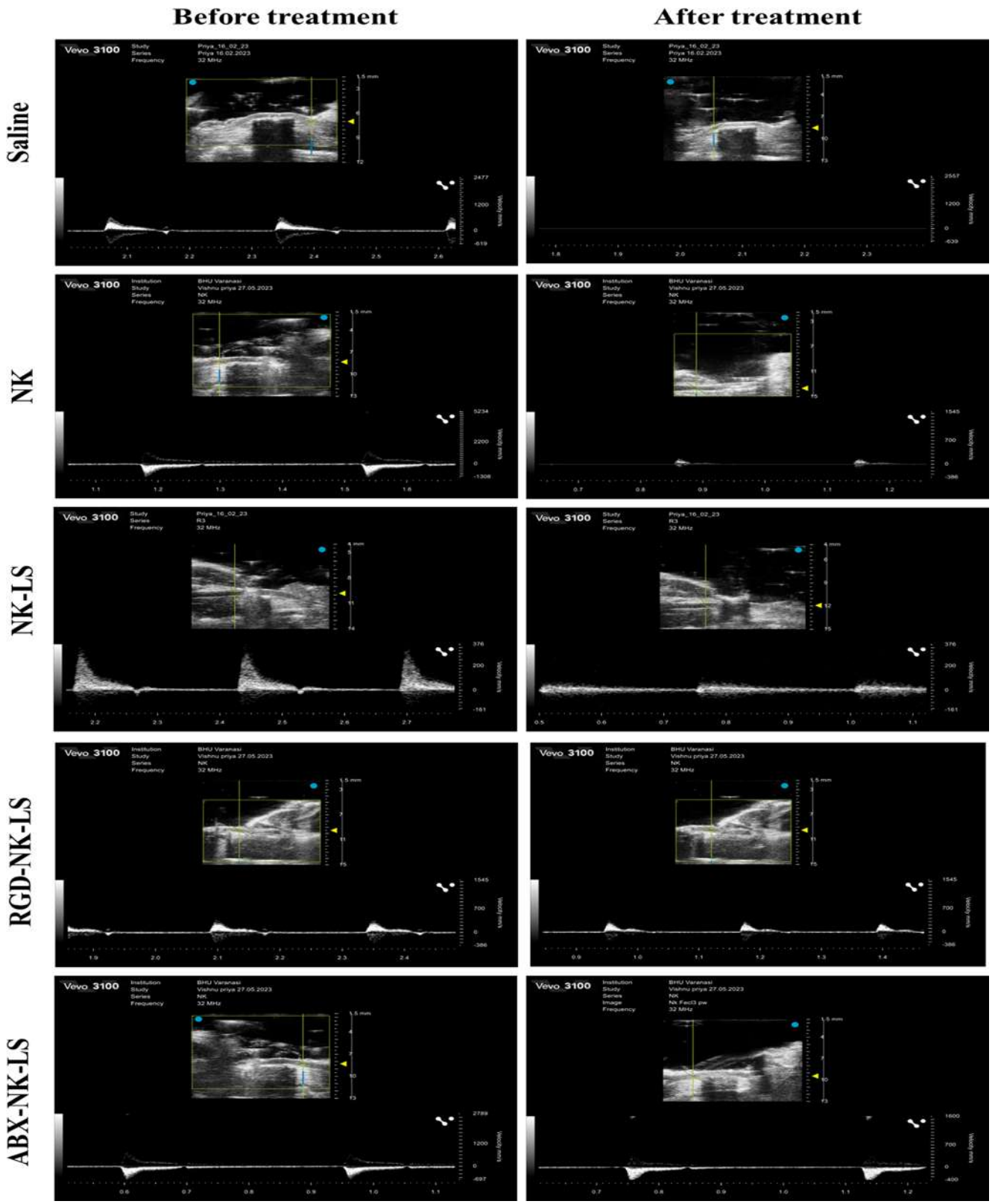

Figure 8. Ultrasound imaging of CA in rats: before and after treatment with $FeCl_3$ and NK, NK-LS, RGD-NK-LS, and AM-NK-LS (each group, $n = 3$ animals).

calculated as 0.89 ± 0.18, 19.81 ± 1.99, 24.49 ± 3.16, 75.5 ± 2.41, and 72.62 ± 2.00%, respectively, as presented in Figure S6.

3.3.5. In Vivo Targeting Capability by Photoacoustic Imaging (PAI). The extent of targeting efficacy of liposomal formulations was analyzed by the Live unmixing mode of photoacoustic imaging in an *in vivo* rat model. The laser with a wavelength range of 680−970 nm was employed for spectral scanning against photoacoustic active dyes to generate acoustic

https://doi.org/10.1021/acs.molpharmaceut.3c00830
Mol. Pharmaceutics 2024, 21, 283−302

signals, and further signals were detected by an ultrasonic transducer to acquire the photoacoustic images. After selecting a specific spectral unmixing algorithm that contributes or separates out methylene blue signals from other chromophores present within the tissue, the preprocessed photoacoustic images were subjected to perform live unmixing to analyze methylene blue-labeled liposome accumulation at the thrombosed site. The obtained color-coded maps or overlay images are shown in the absence of MB dye in the (green color) case of the control (saline) group, whereas the targeted MB-loaded liposomes indicated enhanced accumulation of liposomes in the area of the thrombus. However, nontargeted liposomes showed a slight presence of green fluorescence local to the thrombus.

3.3.6. Histopathological Assessment. An examination of the potential toxicity of fabricated liposomes was performed by the histopathological investigation of the different major vital organs of the rats. The organs were extracted and stored in formalin until histopathological slide preparation after 14 days of drug or liposome administration via the intravenous route. A bright field microscope was used to observe H&E stained sections of rats' organs (brain, heart, kidney, liver, and lungs at a 10× magnification and presented in Figure S7). No evidence of toxicity was observed in any of the major vital organs.

4. DISCUSSION

When an injury occurs, the ability of blood to form clots is essential for preventing excessive bleeding and for repairing the wound. However, the development of undesirable blood clots (thrombosis) in systemic circulation could result in detrimental effects on a person's health.[62] Thrombus formation contributes to restricted blood flow and subsequently leads to ischemic damage to the heart and brain, which can result in life-threatening cardiocerebrovascular disorders. The advancement in antithrombotic therapies is considered to be of utmost importance due to the significant morbidity and mortality caused by thrombotic ailments. Antithrombotic nanomedicines have achieved tremendous advances in recent years owing to the rapid advancements in biomedical nanotechnology for the diagnosis and management of thrombotic diseases.[63] Previous studies on the delivery of thrombolytic medicines using PEGylated polymer and lipids demonstrated a significant rise in half-life, along with improved safety and stability profiles due to restricted drug degradation.

In recent years, ligand-based active targeting approaches have been extensively explored for nanomedicine-based thrombosis treatment. These approaches use peptide sequences as a ligand of specific receptors that are present at the thrombus site and allows site-specific antithrombotic drug delivery to induce thrombolysis simultaneously decreasing the hemorrhagic complications.[64] A naturally obtained NK has demonstrated its potential as a fibrinolytic medication for thrombotic disorders. The antithrombotic potential of NK can be improved, and stability-related problems can be alleviated using liposomal delivery. In this study, RGD and AM conjugations were used to fabricate NK-loaded nontargeted and targeted liposomes. By precisely delivering antithrombotic medicines at the site of the thrombus, targeted liposomes can reduce side effects while concurrently increasing their efficacy.

The particle size is one of the critical factors that should be carefully monitored because it will eventually affect the pharmacokinetics and dynamics of the liposomes when administered into the circulatory system. According to the findings, fabricated liposomes typically range in size from 160 to 200 nm. The size of the targeted liposomes notably increased ($P < 0.05$), when incorporated with the drug and functionalized with peptides at the surface corresponding to successful drug loading and surface conjugation. The PDI values of all the batches of liposomal formulations were under 0.3 which indicated a narrow size distribution.

The conjugation of RGD and AM was confirmed by the change in the zeta potential of the nanoformulations provided with the shifting of values toward negative charge. The loading of NK into liposomes shifted the zeta potential to a less negative side because it carries a positive charge at 7.4 pH considering its isoelectric point, i.e., 8.6. The C6-loaded liposomes followed the same change in the zeta potential after surface conjugation. However, it showed a more negative zeta potential than other NK-loaded liposomes because no positive function was added in the dye-loaded formulation. Moreover, the existence of a TPGS backbone in the liposomal preparations prolongs the biological half-life and minimizes opsonization. Additionally, the influence of % EE was regarded as one of the key factors that estimate the amount of the drug loaded into the liposomes. As compared to targeted liposomes, the % EE of nontargeted liposomes was somewhat greater, indicating the minor loss of the drug while being made into a targeted formulation. Despite this, the slight variation in % EE exerted no impact on the drug's therapeutic potential.

The fabricated liposomes were found to be spherical in shape, consistently dispersed, and free of surface flaws with no sign of rupture and leakage, as shown by the SEM and TEM pictures in Figures 2A and 2B. The liposome's average diameter was in the range of 125−130 nm, while some of them had a lower and larger size distribution. Additionally, the targeted formulation showed a slight increase in particle size, which was in perfect accord with the values of the particle size analyzer. The 3D image of AFM analysis showed a uniform distribution of liposomes.

The Bradford assay demonstrated the presence of targeted moieties (RGD and AM) on the surface of liposomes. Compared to AM-conjugated liposomes, those with RGD decoration demonstrated greater conjugation, possibly as a result of the MABs' larger size, which caused steric hindrance and limited the surface binding to the liposomes. Results, meanwhile, seemed to indicate that the modest conjugation of AM had no significant effect on the targeting potential of liposomes.

Additionally, high-resolution XPS analysis of nontargeted and targeted liposomes was performed to confirm the successful conjugation of the targeting peptides. The surface chemistry analysis showed a relative increase in the atomic percentage of nitrogen (N 1s) after RGD (3.54%) or AM (4.33%) decoration when compared with NK-LS (1.98%). The rise in nitrogen content suggested the presence of AM/RGD on the surface of the liposomal formulation as peptides and MABs are described as nitrogen-rich molecules (Figure 3C). Moreover, in the case of a targeted formulation, the atomic percentage of C 1s was shown to decline, revealing a successful sheathing of the carbon backbone of HSPC-constituted liposomes by surface conjugation. On the other hand, the atomic % of O 1s also seemed to increase when fabricated as targeted liposomes (i.e., for RGD-NK-LS 12.82% and for AM-NK-LS 13.72%) in comparison with nontargeted liposomes (11.61%), suggesting the attachment of oxygen-rich peptides at the liposomal surface.

https://doi.org/10.1021/acs.molpharmaceut.3c00830
Mol. Pharmaceutics 2024, 21, 283−302

The amorphous nature of NK was revealed by XRD spectral examination, which shows a broad peak at a 10°−30° angle. Similarly, the other excipients such as TPGS and HSPC showed widened peaks corresponding to their amorphous nature other than CHOL which showed sharply resolved peaks representing their crystallinity. Additionally, both targeted and nontargeted liposomes showed several minor diffuse peaks appeared in their XRD spectra (Figure 3A). However, the distinctive XRD peaks of NK, CHOL, HSPC, and TPGS were completely dissolved when formulated as liposomes, providing the idea of effective encapsulation and drug loading into the nanovesicles.

TGA analysis was employed to assess the thermal integrity of the components of liposomes and NK-LS with regard to the weight change. Here, the variation in sample weights over a temperature range (25−500 °C) was established. The compound stability attributes at various temperatures were discovered by calculating the weight loss %. NK showed a sudden decline in weight near 200 °C; however, in the case of NK-LS, the decline in weight was in a progressive manner ensuring NK stability in the liposomes. Moreover, other excipients' stability, including TPGS, CHOL, and, HSPC, had been discovered to be enhanced, since prior to the formulation they were showing a quick reduction in mass; however, when they were formulated as NK-LS, the weight loss was minimized and decelerated over a range of temperatures.

The *in vitro* drug release of NK-LS, RGD-NK-LS, and AM-NK-LS was carried out using the sample separation technique in pH 7.4 PBS. The overall CPR of NK from nontargeted liposomes (83.96 ± 2.05) was shown to be higher than RGD-NK-LS (80.3 ± 2.94) and AM-NK-LS (77.96 ± 1.24) at the final time point of 72 h. In addition, the sustained release profile of targeted liposomes was maintained more adequately as compared to nontargeted liposomes up to 72 h, and there was no evidence of a burst release having been observed in any of the liposomal formulations (Figure 4A).

To assess the thrombolytic activity of NK, nontargeted liposomes, and targeted liposomes, an *in vitro* clot lysis investigation was performed. Targeted liposomes showed potent thrombolytic activity in terms of % clot lysis when compared with NK and NK-LS, due to the effect of surface conjugation (AM or RGD) which provides selective binding to GP IIb/IIIa receptors available at the thrombus site. The images were captured at different time intervals revealing the sustained release of NK from liposomal vesicles as the lysis progresses until the last observation point at 12 h, but in the case of free drug, lysis stopped at the initial 4 h showing less efficacy and potency than NK-LS, RGD-NK-LS, and AM-NK-LS.

Additionally, significant changes in the findings of the aPTT and PT values were observed when the coagulation times of the two groups, saline, and NK were compared (Figure 4C,D). The findings support the earlier reported outcomes of research that confirm the increase in aPTT and PT figures when administered with NK. Nontargeted liposomes showed a nonsignificant decrease in aPTT and PT values than NK as it had demonstrated a sustained release profile. Despite this, the PT and aPTT for targeted liposomes were prolonged as compared to saline, NK, and NK-LS groups confirms their strong antithrombotic activity by intrinsic and extrinsic coagulation cascade. Moreover, this increase in aPTT and PT values might also suggest the possibility of synergism.

In further *in vitro* investigations, the therapeutic potential of developed liposomes was determined by estimating the inhibitory efficiency for platelet aggregation. In contrast to free NK and nontargeted liposomes, the targeted liposomes amplify their inhibitory activity and prevent the formation of platelet aggregates more evidently, as shown in Figure 4E. Moreover, it was observed that pure NK possesses significant potential in preventing platelet aggregation. NK-LS demonstrated comparatively less potency toward platelet aggregation than NK due to the sustained release feature suggesting an analogue outcome to aPTT and PT assays. In brief, the platelet aggregation assay demonstrated that AM-NK-LS had greater antithrombotic potential than other liposomal formulations, which may be a result of AM's greater affinity for human integrin receptors.

The blood smears were prepared after incubating liposomal formulations with human blood to investigate the biocompatibility of nanoformulations. The microscopic examination of blood smear slides demonstrated no changes in the morphology of the blood cells (Figure S2A). Furthermore, the hemolytic evaluation of nontargeted and targeted liposomes also proved the safety and biocompatibility of these nanovesicles in human blood. The result demonstrated each of the liposomes exhibited <2% hemolysis and was compatible with biological systems (Figure S2B).

Additionally, the *in vitro* targeting efficacy of C6-LS, C6-RGD-LS, and C6-AM-LS toward activated platelets was evaluated utilizing an imaging device, revealing their affinity as a function of % ROI. The results showed that, as compared to the saline control and nontargeted liposomes, the ROI intensity of targeted liposomes interacted with platelets was significantly greater, referring to their potent affinity toward activated platelets. Figure 5B represents significant differences in % ROI of each group, and C6-AM-LS displayed superior platelet interaction over C6-RGD-LS, which signifies the AM's higher affinity for GP IIb/IIIa receptors.

Similarly, another study was carried out to obtain the platelet binding affinity of liposomal formulations from CLSM studies. It was found that the fluorescence intensity of targeted liposomes (2.329 ± 0.187 and 3.653 ± 0.126% for C6-RGD-LS and C6-AM-LS, respectively) was significantly higher in comparison to free C6 dye (0.663 ± 0.037%) and nontargeted liposomes (0.764 ± 0.088%) when incubated with activated platelets. Additionally, it validates that the GP IIb/IIIa receptors found on the surface of activated platelets specifically interacted with AM or RGD targeted liposomes, as shown in Figures 5C and 5D. Despite the higher magnification, the color intensity of fluorescent picture was found weaker without any cellular uptake. The CLSM images only represent the surface interactions of the liposomes to the activated platelets; therefore, for clear visualization, corresponding binary images were used.

In addition, to validate the *in vitro* fibrinolytic potential of the NK and liposomal formulations, Alexa Fluor 488-labeled thrombus was formed on a fabricated slide. After the addition of test samples, the densely packed fibrin polymers were shown to be lysed significantly when analyzed under CLSM. The fibrin monomers were found to be loosely distributed in the case of NK and other liposomal formulations. However, a significantly higher lysis was observed in the case of AM-NK-LS as compared to other groups. The clot lysis efficacy of nanoformulation was also supported by the values of Z-stack analysis under CLSM which represents the thickness of the fibrinogen layer.

In further investigation, a flow cytometry study was performed to examine the interaction of platelets with nontargeted and targeted liposomes. Here, the platelets were stained with an FL-4 positive antibody, and liposomes loaded with C6 were FL-1 positive; the shift of signal intensity to the fourth quadrant

https://doi.org/10.1021/acs.molpharmaceut.3c00830
Mol. Pharmaceutics 2024, 21, 283−302

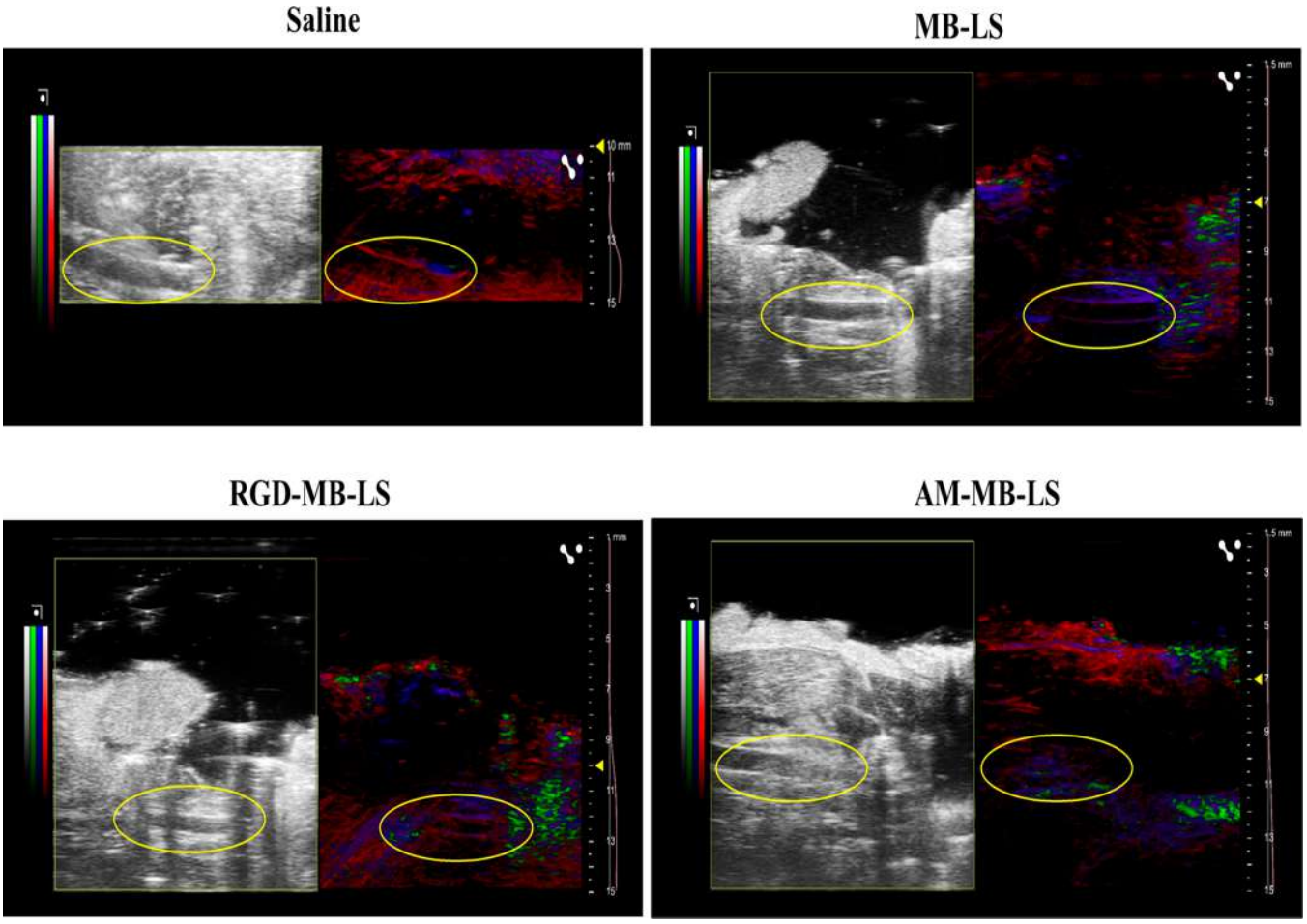

Figure 9. Photoacoustic imaging of the thrombus-induced carotid artery after treatment with saline, MB-LS, RGD-MB-LS, and AM-MB-LS. The circle indicates the area of the thrombus in the carotid artery (each group, n = 3 animals).

signifies the platelet interaction potential of the liposomes. All the liposomal preparations exhibited the fluorescent signal in the fourth quadrant, confirming the platelet interaction. However, a significant increase in signal intensity was observed in the case of targeted liposomes compared to nontargeted liposomes.

By using size distribution analysis in FBS (10% v/v), the stability investigation of NK-LS was carried out. The findings indicated that the size distribution of NK-LS has not changed significantly since after and before incubation, as the curves overlapped without showing any significant change (Figure S4). Additionally, size and PDI measurements were used for the investigation of the stability of NK-LS, RGD-NK-LS, and AM-NK-LS at 4−8 °C, prior to and post 3 months of storage. The obtained particle size and PDI data demonstrated no significant change in the values when stored at 4−8 °C.

Swiss albino mice were used in a tail bleeding assay to test the antithrombotic potency of NK-LS, RGD-NK-LS, and AM-NK-LS. In comparison to free NK, the fabricated liposomes did not exhibit any significant bleeding when administered at lower doses. A subtherapeutic amount of the targeting peptide was used in the targeted liposomes, which reduced the unspecific interactions between platelets and targeting moieties, i.e., RGD and AM. However, due to the immediate availability of NK in the bloodstream after an IV administration, it demonstrated significantly more bleeding than the control group. The targeted liposomal formulation did not show any significant difference in bleeding time, because of the sustained release feature which is consistent with its selectivity toward the occurrence of thrombus and improved antithrombotic ability *in vivo* despite inducing bleeding complications, as presented in Figure 7A.

A clotting time study was carried out to further examine the antithrombotic effects of NK, NK-LS, RGD-NK-LS, and AM-NK-LS using Swiss albino mice. The liposomal formulations demonstrated decreased clotting times when compared to the NK control, which shows that they mitigated the adverse outcomes of NK and were efficient as delivery nanocarriers for NK, as shown in Figure 7B.

Additionally, a study was conducted to demonstrate the *in vivo* thrombolytic efficacy of both nontargeted and targeted liposomes on Sprague−Dawley rats. In comparison to the positive control NK, targeted liposomes showed a significant increase in thrombolysis. However, NK-LS displayed a non-significant difference in thrombolysis with NK as it released the drug in a sustained manner. Moreover, in the case of NK and NK-LS, the thrombolysis was not maintained for a longer duration, whereas targeted liposomes showed consistent and continuous thrombolysis during the study without any significant fall in blood flow after regain. Despite the fact that *in vitro* thrombolysis efficacy was shown to be superior for AM-NK-LS, it exhibits considerably less percent of thrombolysis than RGD-NK-LS in the mentioned *in vivo* rat model which could possibly be indicative of AM moderate affinity for rat integrin receptors.

https://doi.org/10.1021/acs.molpharmaceut.3c00830
Mol. Pharmaceutics 2024, 21, 283−302

Moreover, in another *in vivo* study, an ultrasound imaging system was employed to acquire the ultrasound images and velocity signals of the carotid artery following $FeCl_3$ thrombus formation model protocols with treatment. The ultrasound velocity signals recorded in Power Doppler Mode before and after the treatment demonstrated a significant increase in velocity signals of targeted liposomes as compared to non-targeted liposomes, whereas in the case of saline, the signal totally disappeared indicating complete blockage of the carotid artery without blood flow. AM-NK-LS and RGD-NK-LS showed an increase (≈3 times) in % thrombolysis as compared to nontargeted formulations and showed the efficient restoration of blood flow by dissolving thrombus in the carotid artery of the rats when receiving targeted liposomes (Figure 8). In addition, PAI was also performed to determine the targeting capability of the fabricated liposomes. The photoacoustic images of targeted liposomes (AM-MB-LS and RGD-MB-LS) showed localized accumulation of liposomes within 30 min of treatment following the thrombus, confirming its potent affinity toward the thrombus site that has the activated GPIIb/IIIa receptors. As for nontargeted liposomes, the green fluorescence intensity was much less and nonlocalized to the thrombus indicating their nontargeted profile, as shown in Figure 9.

The toxicity of prepared liposomes on major vital organs of a biological system was assessed, and a histopathology investigation was performed. The findings suggested no toxic lesions or damage after 14 days of intravenous administration of liposomal formulation (Figure S7), which confirms the safety profile of NK-LS, RGD-NK-LS, and AM-NK-LS in a living system.

5. CONCLUSION

In this research, a novel nanotechnology-based approach was proposed for the efficient delivery of NK. NK-loaded liposomes were developed with and without surface conjugation of the targeting substrate. The GP IIb/IIIa receptor antagonists, i.e., RGD (a small tripeptide sequence) and AM (an FDA-approved MAB), were utilized as targeting moieties for thrombus-targeted liposomes. In comparison to pure NK and nontargeted liposomes, the targeted formulations demonstrated higher *in vitro* and *in vivo* potency. *In vivo* experiments showed that all of the liposomal formulations retained NK thrombolytic activity and lengthened the coagulation time through both extrinsic and intrinsic pathways. In contrast to NK, NK-LS not only reduced associated adverse effects such as bleeding but also resolved the issues related to stability, shorter half-life, and bioavailability. Additionally, *in vitro* evaluations utilizing human blood revealed the superior thrombolytic capability of AM-NK-LS over RGD-NK-LS because of its critical affinity for integrin receptors of humans. The *in vivo* experiments were conducted on Sprague–Dawley rats to evaluate thrombolytic effectiveness and targeting capability of AM-NK-LS and RGD-NK-LS, suggesting more potent activity than pure NK in rats. Moreover, the ultrasound imaging and PAI studies successfully demonstrated the localization of targeted liposomes in the vicinity of the thrombosed area along with restoration of blood flow when treated with targeted liposomal formulation. A hemocompatibility investigation confirmed the safety of NK-LS, RGD-NK-LS, and AM-NK-LS in biological systems. Following detailed clinical investigation, these thrombus-targeted liposomes could be employed for prolonged antithrombotic therapy as they had demonstrated significant preclinical efficacy in thrombosis treatment. Moreover, these liposomal formulations may have an additional benefit in large-scale production as their preparation methods are well established for a decade, which increases the chances of industrial applicability.

Despite these preclinical investigations, other *in vivo* animal studies such as the pharmacokinetic study and the carrageenan-induced thrombotic analysis can be carried out to ensure the safety and efficacy of these NK-loaded liposomes. Additionally, clinical trials should be conducted to verify its effectiveness and therapeutic potential in individuals. Prior to receiving regulatory approval for clinical use, the main side effect concerns such as bleeding, biodegradability, and toxicity should also be addressed.

■ ASSOCIATED CONTENT

Supporting Information

The Supporting Information is available free of charge at https://pubs.acs.org/doi/10.1021/acs.molpharmaceut.3c00830.

> Clot lysis study showing lysis of clot at different time intervals (0, 2, 4, 8, and 12 h); A) Brightfield microscopic images (10 X) and B)% hemolysis of human blood treated with saline, NK, NK-LS, RGD-NK-LS, and AM-NK-LS; Flow cytometry data of A) Unstained platelets, B) Resting platelets, C) C6-LS with platelets, D) C6-RGD-LS with platelets, and E) C6-AM-LS with platelets; Comparative bar diagram representing % regain in blood flow after application of $FeCl_3$ with subsequent treatment of saline, NK, NK-LS, RGD-NK-LS, and AM-NK-LS. These data are indicative of three different sets of experiments, represented as Mean ± SD, where ns ($p \geq 0.05$), ***$p < 0.001$, **$p < 0.01$, and *$p < 0.05$; Bar graph representing % thrombolysis in terms of regain in blood velocity after application of $FeCl_3$ with subsequent treatment with saline, NK, NK-LS, RGD-NK-LS, and AM-NK-LS by ultrasound imaging; Microscopical examination of histopathological samples of rat brain, heart, kidney, liver, and lungs (by H&E staining at 10× magnification) after treatment with saline, NK, NK-LS, RGD-NK-LS, and AM-NK-LS; Particle size and PDI of liposomes after and before 3 months of storage at 4−8 °C (PDF)

■ AUTHOR INFORMATION

Corresponding Author

Madaswamy S. Muthu − *Department of Pharmaceutical Engineering and Technology, IIT (BHU), Varanasi 221005, India*; orcid.org/0000-0001-5805-7921; Phone: +91 9235195928; Email: msmuthu.phe@itbhu.ac.in; Fax: +91 542 2368428

Authors

Vishnu Priya − *Department of Pharmaceutical Engineering and Technology, IIT (BHU), Varanasi 221005, India*

Samridhi − *Department of Pharmaceutical Engineering and Technology, IIT (BHU), Varanasi 221005, India*

Nitesh Singh − *Department of Biochemistry, Institute of Medical Sciences, Banaras Hindu University, Varanasi 221005, India*

Debabrata Dash − *Department of Biochemistry, Institute of Medical Sciences, Banaras Hindu University, Varanasi 221005, India*

Complete contact information is available at: https://pubs.acs.org/10.1021/acs.molpharmaceut.3c00830

https://doi.org/10.1021/acs.molpharmaceut.3c00830
Mol. Pharmaceutics 2024, 21, 283−302

Notes

The authors declare no competing financial interest.

■ ACKNOWLEDGMENTS

The authors are grateful to the Indian Institute of Technology − Banaras Hindu University (IIT-BHU), Varanasi, India for the Institute Research Support grant. The authors also express their gratitude to the Ministry of Education (Government of India) for providing the scholarship in the form of Teaching Assistantship. This research was supported partly by a grant from the Indian Council of Medical Research (ICMR) under the 'Center for Advanced Research' (CAR) scheme. The authors are also grateful to the Central Instrument Facilities (CIF), IIT-BHU, Varanasi, and Sophisticated Analytical & Technical Help Institute (SATHI)-BHU, Varanasi for providing instrumentation facilities.

■ REFERENCES

(1) World Health organization. *Cardiovascular diseases*. 2023. https://www.who.int/health-topics/cardiovascular-diseases#tab=tab_1 (accessed 2023-04-26).

(2) Amini, M.; Zayeri, F.; Salehi, M. Trend analysis of cardiovascular disease mortality, incidence, and mortality-to-incidence ratio: results from global burden of disease study 2017. *BMC public health.* **2021**, *21* (1), 401.

(3) Rout, S. K.; Priya, V.; Mehata, A. K.; Muthu, M. S.; et al. Abciximab coated albumin nanoparticles of rutin for improved and targeted antithrombotic effect. *J. Drug Delivery Sci. Technol.* **2022**, *76*, 103785.

(4) Kawata, H.; Uesugi, Y.; Soeda, T.; Takemoto, Y.; Sung, J. H.; Umaki, K.; Kato, K.; Ogiwara, K.; Nogami, K.; Ishigami, K.; et al. A new drug delivery system for intravenous coronary thrombolysis with thrombus targeting and stealth activity recoverable by ultrasound. *J. Am. Coll. Cardiol.* **2012**, *60* (24), 2550−2557.

(5) Mackman, N.; Bergmeier, W.; Stouffer, G. A.; Weitz, J. I. Therapeutic strategies for thrombosis: new targets and approaches. *Nature reviews. Drug discovery.* **2020**, *19* (5), 333−352.

(6) Feng, R.; Li, J.; Chen, J.; Duan, L.; Liu, X.; Di, D.; Deng, Y.; Song, Y. Preparation and toxicity evaluation of a novel nattokinase-tauroursodeoxycholate complex. *Asian journal of pharmaceutical sciences.* **2018**, *13* (2), 173−182.

(7) Dong, X. Y.; Kong, F. P.; Yuan, G. Y.; Wei, F.; Jiang, M. L.; Li, G. M.; Wang, Z.; Zhao, Y. D.; Chen, H. Optimisation of preparation conditions and properties of phytosterol liposome-encapsulating nattokinase. *Nat. Prod. Res.* **2012**, *26* (6), 548−556.

(8) Bhatt, P. C.; Verma, A.; Al-Abbasi, F. A.; Anwar, F.; Kumar, V.; Panda, B. P. Development of surface-engineered PLGA nanoparticulate-delivery system of Tet1-conjugated nattokinase enzyme for inhibition of Aβ(40) plaques in Alzheimer's disease. *Int. J. Nanomedicine.* **2017**, *12*, 8749−8768.

(9) Ren, L.; Wang, X.; Wu, H.; Shang, B.; Wang, J. Conjugation of nattokinase and lumbrukinase with magnetic nanoparticles for the assay of their thrombolytic activities. *Journal of Molecular Catalysis B: Enzymatic.* **2010**, *62* (2), 190−196.

(10) Huang, M.; Zhang, S. F.; Lü, S.; Qi, T.; Yan, J.; Gao, C.; Liu, M.; Li, T.; Ji, Y. Synthesis of mesoporous silica/polyglutamic acid peptide dendrimer with dual targeting and its application in dissolving thrombus. *J. Biomed. Mater. Res., Part A* **2019**, *107* (8), 1824−1831.

(11) Hsieh, C.-W.; Lu, W.-C.; Hsieh, W.-C.; Huang, Y. P.; Lai, C.-H.; Ko, W.-C. Improvement of the stability of nattokinase using γ-polyglutamic acid as a coating material for microencapsulation. *LWT-Food Science and Technology.* **2009**, *42* (1), 144−149.

(12) Deepak, V.; Pandian, S.; Kalishwaralal, K.; Gurunathan, S. Purification, immobilization, and characterization of nattokinase on PHB nanoparticles. *Bioresour. Technol.* **2009**, *100* (24), 6644−6646.

(13) Kozubek, A.; Gubernator, J.; Przeworska, E.; Stasiuk, M. Liposomal drug delivery, a novel approach: PLARosomes. *Acta Biochim Polym.* **2000**, *47* (3), 639−649.

(14) Nakhaei, P.; Margiana, R.; Bokov, D. O.; Abdelbasset, W. K.; Jadidi, Kouhbanani MA.; Varma, R. S.; Marofi, F.; Jarahian, M.; Beheshtkhoo, N. Liposomes: structure, biomedical applications, and stability parameters with emphasis on cholesterol. *Front. Bioeng. Biotechnol.* **2021**, *9*, 705886.

(15) Kelly, C.; Jefferies, C.; Cryan, S. A. Targeted liposomal drug delivery to monocytes and macrophages. *J. Drug Delivery* **2011**, *2011*, 727241.

(16) Bulbake, U.; Doppalapudi, S.; Kommineni, N.; Khan, W. Liposomal formulations in clinical use: an updated review. *Pharmaceutics.* **2017**, *9* (2), 12.

(17) Kumar, L.; Verma, S.; Vaidya, B. Liposomes for the delivery of streptokinase. *Ther. Delivery* **2017**, *8* (10), 855−866.

(18) Hassanpour, S.; Kim, H. J.; Saadati, A.; Tebon, P.; Xue, C.; van den Dolder, F. W.; Thakor, J.; Baradaran, B.; Mosafer, J.; Baghbanzadeh, A.; de Barros, N. R.; Hashemzaei, M.; Lee, K. J.; Lee, J.; Zhang, S.; Sun, W.; Cho, H. J.; Ahadian, S.; Ashammakhi, N.; Dokmeci, M. R.; Mokhtarzadeh, A.; Khademhosseini, A. Thrombolytic agents: nanocarriers in controlled release. *Small.* **2020**, *16* (40), 2001647.

(19) Li, J.; Cheng, X.; Chen, Y.; He, W.; Ni, L.; Xiong, P.; Wei, M. Vitamin E TPGS modified liposomes enhance cellular uptake and targeted delivery of luteolin: An *in-vivo*/in vitro evaluation. *Int. J. Pharm.* **2016**, *512* (1), 262−272.

(20) Mehata, A. K.; Bharti, S.; Singh, P.; Viswanadh, M. K.; Kumari, L.; Agrawal, P.; Singh, S.; Koch, B.; Muthu, M. S. Trastuzumab decorated TPGS-g-chitosan nanoparticles for targeted breast cancer therapy. *Colloids Surf. B Biointerfaces.* **2019**, *173*, 366−377.

(21) Farooq, M. A.; Xinyu, H.; Jabeen, A.; Ahsan, A.; Seidu, T. A.; Kutoka, P. T.; Wang, B. Enhanced cellular uptake and cytotoxicity of vorinostat through encapsulation in TPGS-modified liposomes. *Colloids Surf. B Biointerfaces* **2021**, *199*, 111523.

(22) Bode, C.; Meinhardt, G.; Runge, M. S.; Freitag, M.; Nordt, T.; Arens, M.; Newell, J. B.; Kübler, W.; Haber, E. Platelet-targeted fibrinolysis enhances clot lysis and inhibits platelet aggregation. *Circulation* **1991**, *84* (2), 805−813.

(23) Vaidya, B.; Agrawal, G. P.; Vyas, S. P. Platelets directed liposomes for the delivery of streptokinase: development and characterization. *Eur. J. Pharm. Sci.* **2011**, *44* (5), 589−594.

(24) Antman, E. M.; Giugliano, R. P.; Gibson, C. M.; McCabe, C. H.; Coussement, P.; Kleiman, N. S.; Vahanian, A. A.; Adgey, A.; Menown, I.; Rupprecht; Van der Wieken, R.; Ducas, J.; Scherer, J.; Anderson, K.; Van de Werf, F.; Braunwald, E. Abciximab facilitates the rate and extent of thrombolysis: results of the thrombolysis in myocardial infarction (TIMI) 14 trial. The TIMI 14 Investigators. *Circulation* **1999**, *99* (21), 2720−2732.

(25) Rashid Iqbal, M. Formulation and characterization of rutin trihydrate liposomes for topical delivery. *Int. J. Pharm. Res.* **2015**, *7* (3), 29−37.

(26) Guo, Y.; Shen, L. X.; Lu, Y. F.; Li, H. Y.; Min, K.; Li, L. F.; Yu, C. Y.; Zheng, X. Preparation of rutin-liposome drug delivery systems and evaluation on their in vitro antioxidant activity. *Chin. Herb. Med.* **2016**, *8* (4), 371−375.

(27) Liu, Y.; Sun, C.; Li, W.; Adu-Frimpong, M.; Wang, Q.; Yu, J.; Xu, X. Preparation and characterization of Syringic acid−loaded TPGS liposome with enhanced oral bioavailability and in vivo antioxidant efficiency. *AAPS PharmSciTech* **2019**, *20*, 98.

(28) Kala, S. G.; Chinni, S. Bioavailability enhancement of vitamin E TPGS liposomes of nintedanib esylate: formulation optimization, cytotoxicity and pharmacokinetic studies. *Drug Deliv. and Transl. Res.* **2022**, *12* (11), 2856−2864.

(29) Agarwal, M.; Agarwal, M. K.; Shrivastav, N.; Pandey, S.; Das, R.; Gaur, P. Preparation of chitosan nanoparticles and their in-vitro characterization. *Int. J. Life Sci. Res.* **2018**, *4* (2), 1713−1720.

(30) Smith, M. C.; Crist, R. M.; Clogston, J. D.; McNeil, S. E. Zeta potential: a case study of cationic, anionic, and neutral liposomes. *Anal. Bioanal. Chem.* **2017**, *409*, 5779−5787.

(31) Burande, A. S.; Viswanadh, M. K.; Jha, A.; Mehata, A. K.; Shaik, A.; Agrawal, N.; Poddar, S.; Mahto, S. K.; Muthu, M. S. EGFR targeted

https://doi.org/10.1021/acs.molpharmaceut.3c00830
Mol. Pharmaceutics 2024, 21, 283−302

paclitaxel and piperine co-loaded liposomes for the treatment of triple negative breast cancer. *AAPS. Pharm.Sci.Technol.* **2020**, *21* (5), 151.
(32) Agrawal, P.; Singh, R. P.; Kumari, L.; Sharma, G.; Koch, B.; Rajesh, C. V.; Mehata, A. K.; Singh, S.; Pandey, B. L.; Muthu, M. S.; et al. TPGS-chitosan cross-linked targeted nanoparticles for effective brain cancer therapy. *Mater. Sci. Eng. C Mater. Biol. Appl.* **2017**, *74*, 167−176.
(33) Baxa, U. Imaging of liposomes by transmission electron microscopy. *Characterization of nanoparticles intended for drug delivery.* **2018**, *1682*, 73−88.
(34) Ruozi, B.; Tosi, G.; Leo, E.; Vandelli, M. A. Application of atomic force microscopy to characterize liposomes as drug and gene carriers. *Talanta* **2007**, *73* (1), 12−22.
(35) Vikas; Viswanadh, M. K.; Mehata, A. K.; Sharma, V.; Priya, V.; Varshney, N.; Mahto, S. K.; Muthu, M. S. Bioadhesive chitosan nanoparticles: Dual targeting and pharmacokinetic aspects for advanced lung cancer treatment. *Carbohydr. Poly.* **2021**, *274*, 118617.
(36) Karn, P. R.; Jin, S.-E.; Lee, B. J.; Sun, B. K.; Kim, M. S.; Sung, J. H.; Hwang, S. J. Preparation and evaluation of cyclosporin A-containing proliposomes: a comparison of the supercritical antisolvent process with the conventional film method. *Int. J. Nanomedicine.* **2014**, *9*, 5079.
(37) Viswanadh, M. K.; Vikas; Jha, A.; Reddy Adena, S. K.; Mehata, A. K.; Priya, V.; Neogi, K.; Poddar, S.; Mahto, S. K.; Muthu, M. S. Formulation and in vivo efficacy study of cetuximab decorated targeted bioadhesive nanomedicine for non-small-cell lung cancer therapy. *Nanomedicine (London)* **2020**, *15* (24), 2345−2367.
(38) Aljihani, S. A.; Alehaideb, Z.; Alarfaj, R. E.; Alghoribi, M. F.; Akiel, M. A.; Alenazi, T. H.; Al-Fahad, A. J.; Al Tamimi, S. M.; Albakr, T. M.; Alshehri, A.; et al. Enhancing azithromycin antibacterial activity by encapsulation in liposomes/liposomal-N-acetylcysteine formulations against resistant clinical strains of Escherichia coli. *Saudi J. Biol. Sci.* **2020**, *27* (11), 3065−3071.
(39) Kim, Y.; Park, E. J.; Kim, T. W.; Na, D. H. Recent progress in drug release testing methods of biopolymeric particulate system. *Pharmaceutics.* **2021**, *13* (8), 1313.
(40) Waterborg, J. H.; Matthews, H. R. The Lowry method for protein quantitation. *Basic Protein and Peptide Protocols*; Methods Molecular Biology; 1994; pp 7−10,.
(41) Chandrasekaran, S. D.; Vaithilingam, M.; Shanker, R.; Kumar, S.; Thiyur, S.; Babu, V.; Selvakumar, J. N.; Prakash, S. Exploring the in vitro thrombolytic activity of nattokinase from a new strain Pseudomonas aeruginosa CMSS. *Jundishapur. J. Microbiol.* **2015**, *8* (10), No. e23567.
(42) Lin, K. Y.; Lo, J. H.; Consul, N.; Kwong, G. A.; Bhatia, S. N. Self-titrating anticoagulant nanocomplexes that restore homeostatic regulation of the coagulation cascade. *ACS Nano* **2014**, *8* (9), 8776−85.
(43) Darwish, D. A.; Masoud, H. M. M.; Abdel-Monsef, M. M.; Helmy, M. S.; Zidan, H. A.; Ibrahim, M. A. Phospholipase A2 enzyme from the venom of Egyptian honey bee Apis mellifera lamarckii with anti-platelet aggregation and anti-coagulation activities. *J. Genet. Eng. Biotechnol.* **2021**, *19* (1), 10.
(44) Tian, Y.; Zhao, Y.; Zheng, W.; Zhang, W.; Jiang, X. Antithrombotic functions of small molecule-capped gold nanoparticles. *Nanoscale.* **2014**, *6* (15), 8543−8550.
(45) Pan, Y.; Ren, X.; Wang, S.; Li, X.; Luo, X.; Yin, Z. Annexin V-Conjugated Mixed Micelles as a Potential Drug Delivery System for Targeted Thrombolysis. *Biomacromolecules.* **2017**, *18* (3), 865−876.
(46) Wang, X.; Zhang, Q.; Lv, L.; Fu, J.; Jiang, Y.; Xin, H.; Yao, Q. Glioma and microenvironment dual targeted nanocarrier for improved antiglioblastoma efficacy. *Drug. Delivery* **2017**, *24* (1), 1401−1409.
(47) Priya, V.; Vikas; Mehata, A. K.; Jain, D.; Singh, S. K.; Muthu, M. S. Efficient delivery of abciximab using mesoporous silica nanoparticles: In-vitro assessment for targeted and improved antithrombotic activity. *Colloids Surf. B Biointerfaces.* **2022**, *218*, 112697.
(48) Kälvegren, H.; Jönsson, S.; Jonasson, L. Release of matrix metalloproteinases-1 and −2, but not −9, from activated platelets measured by enzyme-linked immunosorbent assay. *Platelets.* **2011**, *22* (8), 572−8.
(49) Priya, V.; Singh, S. K.; Revand, R.; Kumar, S.; Mehata, A. K.; Sushmitha, P.; Mahto, S. K.; Muthu, M. S. GPIIb/IIIa Receptor Targeted rutin loaded liposomes for site-specific antithrombotic effect. *Mol. pharmaceutics.* **2023**, *20* (1), 663−679.
(50) Singh, N.; Varma, A.; Verma, A.; Maurya, B. N.; Dash, D. Relief from vascular occlusion using photothermal ablation of thrombus with a multimodal perspective. *Nano. Research.* **2016**, *9*, 2327−2337.
(51) Chauhan, A. K.; Motto, D. G.; Lamb, C. B.; Bergmeier, W.; Dockal, M.; Plaimauer, B.; Scheiflinger, F.; Ginsburg, D.; Wagner, D. D. Systemic antithrombotic effects of ADAMTS13. *J. Exp. Med.* **2006**, *203* (3), 767−76.
(52) Kulkarni, P. P.; Tiwari, A.; Singh, N.; Gautam, D.; Sonkar, V. K.; Agarwal, V.; Dash, D. Aerobic glycolysis fuels platelet activation: small-molecule modulators of platelet metabolism as anti-thrombotic agents. *Haematologica.* **2019**, *104* (4), 806−818.
(53) Wu, H.; Su, M.; Jin, H.; Li, X.; Wang, P.; Chen, J.; Chen, J. Rutin-Loaded Silver Nanoparticles With Antithrombotic Function. *Frontiers in bioengineering and biotechnology* **2020**, *8*, 598977.
(54) Liu, Y.; Jennings, N. L.; Dart, A. M.; Du, X. J. Standardizing a simpler, more sensitive and accurate tail bleeding assay in mice. *World. J. Exp. Med.* **2012**, *2* (2), 30−6.
(55) García-Manzano, A.; González-Llaven, J.; Lemini, C.; Rubio-Póo, C. Standardization of rat blood clotting tests with reagents used for humans. *Proc. West. Pharmacol. Soc.* **2001**, *44*, 153−5.
(56) Surin, W.; Prakash, P.; Barthwal, M.; Dikshit, M. Optimization of ferric chloride induced thrombosis model in rats: effect of anti-platelet and anti-coagulant drugs. *J. Pharmacol. Toxicol. Methods.* **2010**, *61* (3), 287−291.
(57) Karatas, H.; Erdener, S. E.; Gursoy-Ozdemir, Y.; Gurer, G.; Soylemezoglu, F.; Dunn, A. K.; Dalkara, T. Thrombotic distal middle cerebral artery occlusion produced by topical FeCl(3) application: a novel model suitable for intravital microscopy and thrombolysis studies. *J. Cereb. Blood Flow Metab.* **2011**, *31* (6), 1452−60.
(58) McCarthy, J. R.; Sazonova, I. Y.; Erdem, S. S.; Hara, T.; Thompson, B. D.; Patel, P.; Botnaru, I.; Lin, C. P.; Reed, G. L.; Weissleder, R.; Jaffer, F. A. Multifunctional nanoagent for thrombus-targeted fibrinolytic therapy. *Nanomedicine (Lond).* **2012**, *7* (7), 1017−1028.
(59) Bonnard, T.; Tennant, Z.; Niego, B. E.; Kanojia, R.; Alt, K.; Jagdale, S.; Law, L. S.; Rigby, S.; Medcalf, R. L.; Peter, K.; Hagemeyer, C. E. Novel thrombolytic drug based on thrombin cleavable microplasminogen coupled to a single-chain antibody specific for activated GPIIb/IIIa. *J. Am. Heart Assoc.* **2017**, *6* (2), No. e004535.
(60) Xu, J.; Zhou, J.; Zhong, Y.; Zhang, Y.; Liu, J.; Chen, Y.; Deng, L.; Sheng, D.; Wang, Z.; Ran, H.; Guo, D. Phase transition nanoparticles as multimodality contrast agents for the detection of thrombi and for targeting thrombolysis: in vitro and in vivo experiments. *ACS Appl. Mater. Interfaces.* **2017**, *9* (49), 42525−42535.
(61) Bi, F.; Zhang, J.; Su, Y.; Tang, Y. C.; Liu, J. N. Chemical conjugation of urokinase to magnetic nanoparticles for targeted thrombolysis. *Biomaterials.* **2009**, *30* (28), 5125−5130.
(62) Jeon, C.; Jun, H.; Kim, S.; Song, N.; Yang, M.; Lim, C.; Lee, D. Clot-targeted antithrombotic liposomal nanomedicine containing high content of H(2)O(2)-activatable hybrid prodrugs. *ACS Appl. Mater. Interfaces.* **2023**, *15*, 8999.
(63) Zhao, Z.; Yang, F.; Zhang, X.; Sun, J.; He, Z.; Luo, C. Emerging nanotherapeutics for antithrombotic treatment. *Biomaterials.* **2020**, *255*, 120200.
(64) Priya, V.; Viswanadh, M. K.; Mehata, A. K.; Jain, D.; Singh, S. K.; Muthu, M. S. Targeted nanotherapeutics in the prophylaxis and treatment of thrombosis. *Nanomedicine (London, England).* **2021**, *16* (13), 1153−1176.

https://doi.org/10.1021/acs.molpharmaceut.3c00830
Mol. Pharmaceutics 2024, 21, 283−302